

# Dark Matter and Collider Studies in the Left-Right Symmetric Model with Vector-Like Leptons

Sahar Bahrami<sup>a,1</sup>, Mariana Frank<sup>b,2</sup>, Dilip Kumar Ghosh<sup>c,3</sup>,  
Nivedita Ghosh<sup>c,4</sup>, Ipsita Saha<sup>d,5</sup>

<sup>a</sup> *Department of Physics, McGill University,  
3600 Rue University, Montreal, Quebec, Canada H3A 2T8*

<sup>b</sup> *Department of Physics, Concordia University, 7141 Sherbrooke St. West,  
Montreal, Quebec, Canada H4B 1R6.*

<sup>b</sup> *Department of Theoretical Physics, Indian Association for the Cultivation of Science.  
2A & 2B, Raja S.C. Mullick Road, Kolkata 700032, India*

<sup>c</sup> *Istituto Nazionale di Fisica Nucleare, Sezione di Roma,  
Piazzale Aldo Moro 2, I-00185 Roma, Italy*

## Abstract

In the context of a left-right symmetric model, we introduce one full generation of vector-like lepton doublets (both left and right-handed) together with their mirror doublets. We show that the lightest vector-like neutrino in the model is right-handed, and can serve as the dark matter candidate. We find that the relic density as well as the direct and indirect DM detection bounds are satisfied for a large range of the parameter space of the model. In accordance with the parameter space, we then explore the possibility of detecting signals of the model both at the LHC and the ILC, in the pair production of the associated vector-like charged leptons which decays into final states including dark matter. A comprehensive analysis of signal and backgrounds shows that the signals at the ILC, especially with polarized beams are likely to be visible, even with low luminosity, rendering our model highly predictable and experimentally testable.

---

<sup>1</sup>sahar.bahrami@mail.mcgill.ca

<sup>2</sup>mariana.frank@concordia.ca

<sup>3</sup>tpdkg@iacs.res.in

<sup>4</sup>tpng@iacs.res.in

<sup>5</sup>ipsita.saha@roma1.infn.it

# 1 Introduction

In left-right symmetric models (LRSM), left- and right-handed particles are treated on the same footing. This represents an improvement over the Standard Model (SM) where, instead of providing an explanation for its origin, parity violation is incorporated *ad hoc* into the model. Left-right models assume parity is conserved at high energies, and broken spontaneously at lower energies, providing an alternative to why would nature prefer any left-right discrimination. In addition, these models have several attractive features, such as providing an explanation for matter-antimatter symmetry, and a natural framework for neutrino masses [1–3]. It is reasonable to ask whether these models can accommodate and explain dark matter (DM), another ingredient missing in the SM.

This topic has been previously explored in the context of LRSM. For instance, imposing a discrete  $Z_2 = (-1)^{3(B-L)}$  symmetry, denoted matter parity that survives after the breaking of global  $SO(10)$  into  $SU(3)_c \otimes SU(2)_L \otimes SU(2)_R \otimes U(1)_{B-L}$ . Identifying some representations of  $SO(10)$  as  $Z_2$  even, while others are odd, a possible DM candidate can be accommodated where the scalars belonging to the odd representation would represent the DM candidates [4]. Alternatively, a  $Z_2$  symmetry can also be imposed such as the triplet scalars ( $\Delta_L$  and  $\Delta_R$ ), introduced in the model, will transform under the symmetry as ( $\Delta_L \rightarrow -\Delta_L$ ,  $\Delta_R \rightarrow \Delta_R$ ). Furthermore, setting the vacuum expectation value (VEV) of the left-handed triplet  $\Delta_L^0$  to be zero ( $v_L = 0$ ), the neutral components would become degenerate and stable, and can thus cater possible dark matter candidates. Unfortunately this  $\Delta_L^0$  candidate cannot provide the correct relic density, due to small annihilation cross sections [5]. This problem has been cured by introducing an additional gauge singlet [6]. Leptophilic properties of the decaying left-handed triplet Higgs have been explored to explain enhancements in neutrino-induced muon fluxes [7], and further properties of the gauge singlet have been explored in [6]. LRSM with fermionic dark matter have also been explored [8–10].

Here we shall explore an alternative candidate for dark matter, vector-like neutrinos. Vector-like fermions appear naturally in composite Higgs models, warped extra dimensions, Little Higgs and extended grand unified theories. In left-right models, where left and right chiral representations are naturally connected, vector-like fermions are germane, as they are characterized by having left- and right-handed components transforming in the same way under the symmetry group of the theory, and by the fact that the couplings for the right-handed components are the same as for the left-handed ones. Vector-like fermions have received much attention lately, being put forth as explanations for hints of new physics at the LHC: the ATLAS diboson [11], the CMS  $eejj$  excess [12] and the 750 GeV diphoton signal [13, 14]. In particular, vector-like particles in the context of left-right symmetric models are inherent in warped space extra dimensional models. If the additional dimension, extending between two branes, one at the TeV scale (IR brane) and the other at Planck scale (UV brane), with

gravity propagating in the bulk, is warped, the resulting geometry generates naturally the hierarchy between the electroweak scale ( $M_{\text{ew}} \sim 200$  GeV) and the Planck scale ( $M_{\text{Pl}} \sim 10^{18}$  GeV) [15, 16]. In addition if one allows the SM fields to propagate in the bulk of the fifth dimension, these models can explain the observed masses of the fermions, with lighter fermions localized near the Planck brane and the heavier ones localized near the TeV brane. Within this new framework, generic models with warped extra dimensions are still very constrained by electroweak and flavor precision tests [17]. To reduce the pressure from electroweak precision tests, a common cure is to enlarge the gauge symmetry of the SM by introducing a custodial  $SU(2)_L \times SU(2)_R$  symmetry that limits the corrections to various precision observables [18]. This new symmetry provides a natural framework for vector-like fermions in LRSM, which appear as KK excitations of SM chiral fermions.

Vector-like fermions appear in LRSM also from gauged flavor symmetries, where they are needed to cancel new gauge anomalies [19]. Additionally, in left-right models the scale where the parity breaks down,  $\Lambda_R$  is expected to be high,  $10^{14}$  GeV or higher. One could introduce another intermediate mass scale, associated with  $B - L$  breaking scale  $\Lambda_{B-L}$  [20], which could emerge as the scale of some new fermions, in our case the vector-like leptons, sometimes interpreted as the scale of compositeness [21]. In addition, it is known that in two-Higgs doublet models, vector-like fermions, in addition to the extra Higgs bosons, alleviate electroweak precision tests [22].

Effects of vector-like fermions to the couplings of the SM-like 125 GeV Higgs boson, constrained from measurements of the Higgs production cross-sections and branching ratios at LHC have been analyzed before [23]. Here we examine the possibility that, in the context of LRSM, when they can become dark matter candidates, what is their effect on the parameter space, and how can this scenario be discriminated at the present (LHC) and proposed (ILC) colliders.

Our work is organized as follows. In Section 2 we describe the LRSM with the addition of vector-like lepton doublets. For simplicity, we concentrate in particular on scenarios where mixing between ordinary leptons and vector-like leptons are forbidden by a discrete parity symmetry. The model has one left-handed and one right-handed doublet, and their mirrors representations, yielding mixing between same charge components. We discuss the mass eigenstates, the lightest of which would be the dark matter candidate. In Section 3 we calculate the relic density, the spin-independent and spin-dependent cross sections, the annihilation cross section and muon and neutrino fluxes, and explore the parameter space which is consistent with the experimental results on dark matter detection. In Section 4 we explore ways in which this scenario can be tested, in particular, looking for signals of the lightest vector-like charged lepton pair at the LHC (4.2) and ILC (4.3). We summarize our results in Section 5. In the Appendix we provide explicit expressions for the vector-like lepton mass eigenstates.

## 2 The left-right symmetric model

In the left-right symmetric model [1–3], the Standard Model gauge symmetry is extended to include the gauge group  $SU(2)_R$  (with gauge coupling  $g_R$ ). All right-handed fermions are doublets under this gauge group. Below we give their quantum numbers under  $SU(2)_L \otimes SU(2)_R \otimes U(1)_{B-L}$ . The ordinary fermions are: the leptons

$$L_{Li} = \begin{pmatrix} \nu_L \\ \ell_L \end{pmatrix}_i \sim (\mathbf{2}, \mathbf{1}, -1), \quad L_{Ri} = \begin{pmatrix} \nu_R \\ \ell_R \end{pmatrix}_i \sim (\mathbf{1}, \mathbf{2}, -1), \quad (1)$$

and the quarks

$$Q_{Li} = \begin{pmatrix} u_L \\ d_L \end{pmatrix}_i \sim (\mathbf{2}, \mathbf{1}, \mathbf{1/3}), \quad Q_{Ri} = \begin{pmatrix} u_R \\ d_R \end{pmatrix}_i \sim (\mathbf{1}, \mathbf{2}, \mathbf{1/3}), \quad (2)$$

where  $i = 1, 2, 3$  are generation indices. Note that the right-handed neutrino is automatically included. The electroweak symmetry is broken by the bi-doublet Higgs field

$$\Phi \equiv \begin{pmatrix} \phi_1^0 & \phi_2^+ \\ \phi_1^- & \phi_2^0 \end{pmatrix} \sim (\mathbf{2}, \mathbf{2}, \mathbf{0}). \quad (3)$$

In addition, to break the  $SU(2)_R \otimes U(1)_{B-L}$  gauge symmetry and to provide Majorana mass terms for neutrinos we introduce the Higgs triplets

$$\Delta_L \equiv \begin{pmatrix} \delta_L^+/\sqrt{2} & \delta_L^{++} \\ \delta_L^0 & -\delta_L^+/\sqrt{2} \end{pmatrix} \sim (\mathbf{3}, \mathbf{1}, \mathbf{2}), \quad \Delta_R \equiv \begin{pmatrix} \delta_R^+/\sqrt{2} & \delta_R^{++} \\ \delta_R^0 & -\delta_R^+/\sqrt{2} \end{pmatrix} \sim (\mathbf{1}, \mathbf{3}, \mathbf{2}). \quad (4)$$

The electric charge is given by  $Q = T_L^3 + T_R^3 + \frac{B-L}{2}$ . The subscripts  $L$  and  $R$  are associated with the projection  $P_{L,R} = \frac{1}{2}(1 \mp \gamma_5)$ . We add one family of vector-like leptons<sup>6</sup>

$$\begin{aligned} L'_L &= \begin{pmatrix} \nu'_L \\ \ell'_L \end{pmatrix} \sim (\mathbf{2}, \mathbf{1}, -1), & L'_R &= \begin{pmatrix} \nu'_R \\ \ell'_R \end{pmatrix} \sim (\mathbf{1}, \mathbf{2}, -1), \\ L''_R &= \begin{pmatrix} \nu''_R \\ \ell''_R \end{pmatrix} \sim (\mathbf{2}, \mathbf{1}, -1), & L''_L &= \begin{pmatrix} \nu''_L \\ \ell''_L \end{pmatrix} \sim (\mathbf{1}, \mathbf{2}, -1), \end{aligned} \quad (5)$$

---

<sup>6</sup>Vector-like quarks can also appear; for the present work, we assume them much heavier than the leptons, based on the mass limits [24] and thus they decouple from the low energy spectrum.

where  $L'_L$  and  $L'_R$  are new fermion doublets and  $L''_R$  and  $L''_L$  are the mirror doublets. Furthermore, using the gauge symmetry to eliminate complex phases, the most general vacuum is

$$\langle \Phi \rangle = \begin{pmatrix} \kappa_1/\sqrt{2} & 0 \\ 0 & \kappa_2 e^{i\alpha}/\sqrt{2} \end{pmatrix}, \quad \langle \Delta_L \rangle = \begin{pmatrix} 0 & 0 \\ v_L e^{i\theta_L}/\sqrt{2} & 0 \end{pmatrix}, \quad \langle \Delta_R \rangle = \begin{pmatrix} 0 & 0 \\ v_R/\sqrt{2} & 0 \end{pmatrix}. \quad (6)$$

Note that only  $\Delta_R$  is needed for symmetry breaking, and  $\Delta_L$  is included to preserve left-right symmetry. The Lagrangian density for this model contains, in addition to the SM terms, kinetic, Yukawa for ordinary leptons, explicit terms for the vector-like leptons, and potential terms:

$$\mathcal{L}_{\text{LRM}} = \mathcal{L}_{\text{kin}} + \mathcal{L}_Y + \mathcal{L}_{\text{VL}} - V(\Phi, \Delta_L, \Delta_R), \quad (7)$$

where

$$\begin{aligned} L_{\text{kin}} &= i \sum \bar{\psi} \gamma^\mu D_\mu \psi = \bar{L}'_L \gamma^\mu \left( i \partial_\mu + g_L \frac{\vec{\tau}}{2} \cdot \vec{W}_{L\mu} - \frac{g'}{2} B_\mu \right) L'_L \\ &+ \bar{L}'_R \gamma^\mu \left( i \partial_\mu + g_R \frac{\vec{\tau}}{2} \cdot \vec{W}_{R\mu} - \frac{g'}{2} B_\mu \right) L'_R + \bar{L}''_L \gamma^\mu \left( i \partial_\mu + g_L \frac{\vec{\tau}}{2} \cdot \vec{W}_{L\mu} - \frac{g'}{2} B_\mu \right) L''_L \\ &+ \bar{L}''_R \gamma^\mu \left( i \partial_\mu + g_L \frac{\vec{\tau}}{2} \cdot \vec{W}_{L\mu} - \frac{g'}{2} B_\mu \right) L''_R, \end{aligned} \quad (8)$$

where we introduce the gauge fields,  $\vec{W}_{L,R}$  and  $B$  corresponding to  $SU(2)_{L,R}$  and  $U(1)_{B-L}$ . They mix with the following matrices [25]

$$\begin{pmatrix} W_L^\pm \\ W_R^\pm \end{pmatrix} = \begin{pmatrix} \cos \xi & \sin \xi e^{i\alpha} \\ -\sin \xi e^{-i\alpha} & \cos \xi \end{pmatrix} \begin{pmatrix} W_1^\pm \\ W_2^\pm \end{pmatrix}. \quad (9)$$

The angle  $\xi$  characterizes the mixing between left- and right-handed gauge bosons, with  $\tan 2\xi = -\frac{2\kappa_1\kappa_2}{v_R^2 - v_L^2}$ . Assuming that  $\kappa_2 < \kappa_1$ , it follows that

$$\xi \simeq -\kappa_1\kappa_2/v_R^2 \simeq -2\frac{\kappa_2}{\kappa_1} \left( \frac{m_{W_L}}{m_{W_R}} \right)^2, \quad (10)$$

so that the mixing angle  $\xi$  is at most<sup>7</sup> the square of the ratio of left and right scales  $(\Lambda_L/\Lambda_R)^2$ . Here  $\Lambda_L \simeq 10^2$  GeV corresponds to the electroweak scale and  $\Lambda_R \simeq$  TeV is the scale of parity breaking,  $v_R$ .

With negligible mixing the gauge boson masses become, for  $g_L = g_R$ ,

$$m_{W_L} \simeq m_{W_1} \simeq \frac{g}{2} \kappa_+, \quad \text{and} \quad m_{W_R} \simeq m_{W_2} \simeq \frac{g}{\sqrt{2}} v_R, \quad (11)$$

<sup>7</sup>Although the experimental limit is  $\xi < 10^{-2}$  [24], for  $m_{W_R} = \mathcal{O}(\text{TeV})$  one has  $\xi \leq 10^{-3}$  [26]; supernova bounds for right-handed neutrinos lighter than 1 MeV are even more stringent ( $\xi < 3 \times 10^{-5}$ ) [26, 27].

with  $\kappa_+^2 = \kappa_1^2 + \kappa_2^2$ . The model also has an additional neutral gauge boson,  $Z_R$ , which mixes with the standard model  $Z$  boson. The mass eigenstates  $Z_{1,2}$  acquire masses

$$m_{Z_1} \simeq \frac{g}{2 \cos \theta_W} \kappa_+ \simeq \frac{m_{W_1}}{\cos \theta_W}, \quad \text{and} \quad m_{Z_2} \simeq \frac{g \cos \theta_W}{\sqrt{\cos 2\theta_W}} v_R \simeq \sqrt{\frac{2 \cos^2 \theta_W}{\cos 2\theta_W}} m_{W_2}, \quad (12)$$

where  $g = e/\sin \theta_W$  and with the  $U(1)_{B-L}$  coupling constant  $g_{B-L} \equiv e/\sqrt{\cos 2\theta_W}$ . Again one expects the mixing between the neutral gauge bosons to be of order  $(\Lambda_L/\Lambda_R)^2$ , i.e.,

$$\sin 2\phi = -\frac{g^2 \kappa_+^2 \sqrt{\cos 2\theta_W}}{2c_W^2 (m_{Z_2}^2 - m_{Z_1}^2)} \simeq -\frac{2m_{Z_1}^2 \sqrt{\cos 2\theta_W}}{m_{Z_2}^2 - m_{Z_1}^2} \simeq -2\sqrt{\cos 2\theta_W} \left( \frac{m_{Z_1}}{m_{Z_2}} \right)^2. \quad (13)$$

Eqs. (11) and (12) imply that  $m_{Z_2} \simeq 1.7m_{W_2}$ . The appropriate gauge coupling constants are  $g_s$ ,  $g_L = g_R$  and  $g' = g_{B-L}$ , respectively. The right handed  $SU(2)_R$  breaking scale is restricted from low energy observables, such as  $K_L - K_S$ ,  $\epsilon_K$ ,  $B^0 - \bar{B}^0$  mixings and  $b \rightarrow s\gamma$  processes where the right handed charged current contributes significantly [25, 28–37]. Thus, these processes provide a bound to the scale  $v_R$  by means of charged right handed  $W_R$  boson mass as well as the LR Higgs masses. In particular, the right handed  $W_R$  mass is restricted to be greater than 3 TeV while the heavy bi-doublet Higgs mass should at least be 10 TeV [25]. In our study, we thus fix the scale  $v_R$  at 10 TeV.

The rest of the Lagrangian terms

$$\begin{aligned} \mathcal{L}_Y = & - \left[ Y_L \bar{L}_L \Phi L_R + Y_R \bar{L}_R \Phi L_L + \tilde{Y}_L \bar{L}_L \tilde{\Phi} L_R + \tilde{Y}_R \bar{L}_R \tilde{\Phi} L_L \right. \\ & \left. + h_{L_{ij}} \bar{L}_L^c i\tau_2 \Delta_L L_L + h_{R_{ij}} \bar{L}_R^c i\tau_2 \Delta_R L_R + \text{h.c.} \right] \end{aligned} \quad (14)$$

are the Yukawa interaction terms for the ordinary leptons, with  $Y_{L,R}$ ,  $\tilde{Y}_{L,R}$  and  $Y_{Q_{L,R}}$ ,  $\tilde{Y}_{Q_{L,R}}$   $3 \times 3$  complex matrices, and  $h_{L_{ij}}$ ,  $h_{R_{ij}}$   $3 \times 3$  complex symmetric Yukawa matrices and  $\tilde{\Phi} = \tau_2 \Phi^* \tau_2$ . Additionally, with the vector-like family of leptons as defined above, the Lagrangian describing Yukawa interaction terms for vector-like fermions and their interactions with ordinary fermions, and allowing for both Dirac and Majorana mass terms, is

$$\begin{aligned} \mathcal{L}_{\text{VL}} = & - \left[ M_L \bar{L}'_L L''_R + M_R \bar{L}'_R L''_L + Y'_L \bar{L}'_L \Phi L'_R + Y'_R \bar{L}'_R \Phi L''_L + \tilde{Y}'_L \bar{L}'_L \tilde{\Phi} L'_R + \tilde{Y}'_R \bar{L}'_R \tilde{\Phi} L''_L \right. \\ & + h'_L \bar{L}'_L i\tau_2 \Delta_L L'_L + h''_R \bar{L}'_R i\tau_2 \Delta_R L''_L + h'_R \bar{L}'_R i\tau_2 \Delta_R L'_L + h''_L \bar{L}'_L i\tau_2 \Delta_L L''_R + \lambda'_L \bar{L}'_L \Phi L'_R \\ & \left. + \lambda'_R \bar{L}'_R \tilde{\Phi} L'_R + \lambda''_L \bar{L}'_L i\tau_2 \Delta_L L'_L + \lambda''_R \bar{L}'_R i\tau_2 \Delta_R L'_L + \lambda''_L \bar{L}'_L i\tau_2 \Delta_L L''_R + \lambda''_R \bar{L}'_R i\tau_2 \Delta_R L''_L + \text{h.c.} \right] \end{aligned} \quad (15)$$

Here, in addition to the new Yukawa couplings  $Y'_{L,R}$ ,  $Y''_{L,R}$  of the vector-like leptons with the bidoublet, and  $h'_{L,R}$ ,  $h''_{L,R}$ , the Yukawa couplings of the vector-like leptons with triplet  $\Delta_{L,R}$ , we also introduced

explicit mass terms for the vector-like leptons  $M_L$  and  $M_R$ . The scalar potential for the bidoublet  $\Phi$  and triplet  $\Delta_{L,R}$  Higgs fields is

$$\begin{aligned}
V(\phi, \Delta_L, \Delta_R) = & -\mu_1^2 \left( \text{Tr} [\Phi^\dagger \Phi] \right) - \mu_2^2 \left( \text{Tr} [\tilde{\Phi} \Phi^\dagger] + \left( \text{Tr} [\tilde{\Phi}^\dagger \Phi] \right) \right) - \mu_3^2 \left( \text{Tr} [\Delta_L \Delta_L^\dagger] + \text{Tr} [\Delta_R \Delta_R^\dagger] \right) \\
& + \lambda_1 \left( \left( \text{Tr} [\Phi \Phi^\dagger] \right)^2 \right) + \lambda_2 \left( \left( \text{Tr} [\tilde{\Phi} \Phi^\dagger] \right) + \left( \text{Tr} [\tilde{\Phi}^\dagger \Phi] \right) \right)^2 + \lambda_3 \left( \text{Tr} [\tilde{\Phi} \Phi^\dagger] \text{Tr} [\tilde{\Phi}^\dagger \Phi] \right) \\
& + \lambda_4 \left( \text{Tr} [\Phi \Phi^\dagger] \left( \text{Tr} [\tilde{\Phi} \Phi^\dagger] + \text{Tr} [\tilde{\Phi}^\dagger \Phi] \right) \right) + \rho_1 \left( \left( \text{Tr} [\Delta_L \Delta_L^\dagger] \right)^2 + \left( \text{Tr} [\Delta_R \Delta_R^\dagger] \right)^2 \right) \\
& + \rho_2 \left( \text{Tr} [\Delta_L \Delta_L] \text{Tr} [\Delta_L^\dagger \Delta_L^\dagger] + \text{Tr} [\Delta_R \Delta_R] \text{Tr} [\Delta_R^\dagger \Delta_R^\dagger] \right) \\
& + \rho_3 \left( \text{Tr} [\Delta_L \Delta_L^\dagger] \text{Tr} [\Delta_R \Delta_R^\dagger] \right) + \rho_4 \left( \text{Tr} [\Delta_L \Delta_L] \text{Tr} [\Delta_R^\dagger \Delta_R^\dagger] + \text{Tr} [\Delta_L^\dagger \Delta_L^\dagger] \text{Tr} [\Delta_R \Delta_R] \right) \\
& + \alpha_1 \left( \text{Tr} [\Phi \Phi^\dagger] \left( \text{Tr} [\Delta_L \Delta_L^\dagger] + \text{Tr} [\Delta_R \Delta_R^\dagger] \right) \right) \\
& + \alpha_2 \left( \text{Tr} [\Phi \tilde{\Phi}^\dagger] \text{Tr} [\Delta_R \Delta_R^\dagger] + \text{Tr} [\Phi^\dagger \tilde{\Phi}] \text{Tr} [\Delta_L \Delta_L^\dagger] \right) \\
& + \alpha_2^* \left( \text{Tr} [\Phi^\dagger \tilde{\Phi}] \text{Tr} [\Delta_R \Delta_R^\dagger] + \text{Tr} [\tilde{\Phi}^\dagger \Phi] \text{Tr} [\Delta_L \Delta_L^\dagger] \right) \\
& + \alpha_3 \left( \text{Tr} [\Phi \Phi^\dagger \Delta_L \Delta_L^\dagger] + \text{Tr} [\Phi^\dagger \Phi \Delta_R \Delta_R^\dagger] \right) \\
& + \beta_1 \left( \text{Tr} [\Phi \Delta_R \Phi^\dagger \Delta_L^\dagger] + \text{Tr} [\Phi^\dagger \Delta_L \Phi \Delta_R^\dagger] \right) + \beta_2 \left( \text{Tr} [\tilde{\Phi} \Delta_R \Phi^\dagger \Delta_L^\dagger] + \text{Tr} [\tilde{\Phi}^\dagger \Delta_L \Phi \Delta_R^\dagger] \right) \\
& + \beta_3 \left( \text{Tr} [\Phi \Delta_R \tilde{\Phi}^\dagger \Delta_L^\dagger] + \text{Tr} [\Phi^\dagger \Delta_L \tilde{\Phi} \Delta_R^\dagger] \right), \tag{16}
\end{aligned}$$

where we followed [38] and explicitly indicated the complex parameters. The parameters can be further reduced and simplified by making use of the symmetries of the model. Assuming a discrete left-right symmetry in addition to the left-right gauge symmetry, the  $SU(2)$  gauge couplings become equal ( $g_L = g_R = g$ ) and the Yukawa coupling matrices for the left and right handed sector in the model are related. With a discrete parity symmetry ( $L'_L \leftrightarrow L'_R$ ,  $L''_L \leftrightarrow L''_R$ ,  $\Phi \leftrightarrow \Phi^\dagger$ ,  $\Delta_L \leftrightarrow \Delta_R^*$ ) it follows that  $h'_{L,R} = h''_{L,R}^*$ ,  $Y'_L = Y_L'^*$ ,  $\tilde{Y}_L = \tilde{Y}_L'^*$ ,  $Y'_R = Y_R'^*$ ,  $\tilde{Y}_R = \tilde{Y}_R'^*$ . In addition, using the charge conjugation symmetry we obtain  $h'_{L,R} = h''_{L,R} \equiv h$ . New symmetries can be introduced to restrict the interactions of the vector leptons. For instance, we can impose (i) a symmetry under which all the new  $SU(2)_R$  doublet fields are odd, while the new  $SU(2)_L$  doublets are even, which forces all Yukawa couplings involving new fermions to vanish,  $Y'_L = \tilde{Y}'_L = Y'_R = \tilde{Y}'_R = h'_{L,R} = h''_{L,R} = 0$ , and the vector fermion masses arise only from explicit terms in the Lagrangian [39]; and/or (ii) impose a new parity symmetry which disallows mixing between the ordinary fermions and the new fermion fields, under which all the new vector-like fields are odd, while the others are even [40], such that  $\lambda'^i_L = \lambda''^i_L = \lambda'^i_R = \lambda''^i_R = 0$ . The latter are important for light vector-like leptons, as this scenario would satisfy restrictions from lepton-flavor violating decays, which otherwise would either force the new leptons to be very heavy,  $\sim 10 - 100$  TeV, or else reduce the branching ratio for the Higgs into di-leptons to 30-40% of the SM prediction [40, 41]. Alternatively, one can restrict the mixing of the

vector-like leptons to involve only the third generation ordinary leptons, *i. e.*, the  $\tau$ . In addition, if all vector-like fermions are odd under the  $(ii)$  symmetry, the lightest particle can become stable and act as all, or part of, the dark matter in the universe. Thus in what follows we will perform the analysis under the simplifying assumption  $(ii)$ , and then allow  $\lambda_L^3 = \lambda_R^3 = \lambda_L'^3 = \lambda_R'^3 = \lambda_L''^3 = \lambda_R''^3 \neq 0$  only [42], and see how it affects the phenomenology and collider signals expected in this model.

## 2.1 Vector-like leptons

The spectrum from Eq. 5 now consists of, in the charged sector, a  $2 \times 2$  dimensional mass matrix  $\mathcal{M}_c$

$$(\bar{e}'_L \quad \bar{e}''_L) (\mathcal{M}_c) \begin{pmatrix} e'_R \\ e''_R \end{pmatrix}, \quad \text{with} \quad \mathcal{M}_c = \begin{pmatrix} m'_E & M_L \\ M_R & m''_E \end{pmatrix}, \quad (17)$$

with  $m'_E = \frac{Y_L'^e \kappa_2 e^{i\alpha} + \tilde{Y}_L'^e \kappa_1}{\sqrt{2}}$  and  $m''_E = \frac{Y_R'^e \kappa_2 e^{i\alpha} + \tilde{Y}_R'^e \kappa_1}{\sqrt{2}}$ , from the Lagrangian Eq. (15). The mass matrix can be diagonalized by two unitary matrices  $U^L$  and  $U^R$  as follows:

$$U^{L\dagger} \mathcal{M}_c U^R = \begin{pmatrix} M_{E_1} & 0 \\ 0 & M_{E_2} \end{pmatrix}. \quad (18)$$

The mass eigenvalues are (by convention the order is  $M_{E_1} > M_{E_2}$ )

$$M_{E_1, E_2}^2 = \frac{1}{2} \left[ (M_L^2 + m_E'^2 + M_R^2 + m_E''^2) \pm \sqrt{(M_L^2 + m_E'^2 - M_R^2 - m_E''^2)^2 + 4(m_E'' M_L + m_E' M_R)^2} \right], \quad (19)$$

In the neutral sector the mass matrix is:

$$\frac{1}{2} (\bar{\nu}'_L \quad \bar{\nu}'_R \quad \bar{\nu}''_R \quad \bar{\nu}''_L) (\mathcal{M}_\nu) \begin{pmatrix} \nu_L'^c \\ \nu_R'^c \\ \nu_R''^c \\ \nu_L''^c \end{pmatrix}$$

$$\text{with } \mathcal{M}_\nu = \begin{pmatrix} \sqrt{2} h_L' v_L e^{i\theta} & m'_\nu & M_L & 0 \\ m'_\nu & M'_\nu & 0 & M_R \\ M_L & 0 & \sqrt{2} h_L'' v_L e^{i\theta} & m''_\nu \\ 0 & M_R & m''_\nu & M''_\nu \end{pmatrix}, \quad (20)$$



with Dirac masses  $m'_\nu = \frac{Y_L^{\prime\nu}\kappa_1 + \tilde{Y}_L^{\prime\nu}\kappa_2 e^{-i\alpha}}{\sqrt{2}}$ ,  $m''_\nu = \frac{Y_R^{\prime\nu}\kappa_1 + \tilde{Y}_R^{\prime\nu}\kappa_2 e^{-i\alpha}}{\sqrt{2}}$  and with Majorana masses  $M'_\nu = \sqrt{2}h'_R v_R$  and  $M''_\nu = \sqrt{2}h''_R v_R$ . This mass matrix can be diagonalized by a unitary matrix  $V$ :

$$V^\dagger \mathcal{M}_\nu V = \begin{pmatrix} M_{\nu_1} & 0 & 0 & 0 \\ 0 & M_{\nu_2} & 0 & 0 \\ 0 & 0 & M_{\nu_3} & 0 \\ 0 & 0 & 0 & M_{\nu_4} \end{pmatrix}. \quad (21)$$

Exact analytic expressions are difficult to find<sup>8</sup>. To simplify, we work in the limit where  $h''_R = Y_R^{\prime\nu} = \tilde{Y}_R^{\prime\nu} = 0$  (meaning  $M''_\nu = m''_\nu = 0$ ). Additionally the Yukawa couplings  $Y_L^{\prime\nu}$ ,  $\tilde{Y}_L^{\prime\nu}$  must remain small to insure smallness of couplings to the  $Z_L$  boson. In the limit where  $m'_\nu \ll M_L, M_R$ , the neutrino mass matrix can be diagonalized yielding four neutrino masses:

$$M_{\nu_{1,2}} = \frac{M'_\nu}{2} \mp \sqrt{\frac{M'^2_\nu}{4} + M_R^2 + m'^2_\nu}, \quad (22)$$

$$M_{\nu_{3,4}} = \pm M_L, \quad (23)$$

valid to  $\mathcal{O}(m'^2_\nu/M_L)$ . The lightest of these eigenvalues will be the dark matter candidate, which, as it is odd under the additional parity symmetry (*ii*), it is stable. The lightest eigenvalue will depend on assumptions made on the masses  $M_L, M_R$  and triplet Yukawa couplings  $h'_R$  and  $Y'_L$ . In the limit in which  $M_L \gg M_R$ , there are two heavy (approximately) degenerate eigenvalues of mass  $M_L$ , which do not mix with the lighter states  $\nu_1$  and  $\nu_2$ . In this limit, the lightest state is  $\nu_1$ , and it is mostly the  $\nu_L''$  state, with some admixture of  $\nu_R^c$ , and is right-handed.

Some comments about this analysis:

- If we required  $M'_\nu = m'_\nu = 0$  instead of  $M''_\nu = m''_\nu = 0$ , there is no difference in the final result, but we have  $m''_\nu$  in the mass expressions replacing  $m'_\nu$ .
- If we set  $M'_\nu = m'_\nu = 0$  we flip between the  $'$  and the  $''$  states and the lightest vector-like neutrino will be  $\nu_L'$ .
- The states with mass  $\pm M_L$  are unaffected by Yukawa couplings and thus they are not a good choice for a DM candidate.
- It is advantageous that we get a right-handed neutrino to be the DM candidate, as it is more likely to produce a relic density in the desired range.

---

<sup>8</sup>In our analyses, we use exact numerical expressions, and show here approximate analytical expressions for clarity.

We now explore the parametric dependence of heavy vector-like leptons in this model. While varying some of the parameters, we fix other parameters mostly to values that we choose as benchmark points in our following studies. We shall discuss the benchmark points and corresponding parameters in a later section.

In Figs. 1 and 2 we show the mass dependence of the charged vector-like leptons (both  $E_2$  and  $E_1$ ) on the various parameters of the model. Specifically, we show the contour plots of  $M_{E_2}$  and  $M_{E_1}$  in the  $(M_L, M_R)$  plane and in the planes correlating  $M_L$  and  $M_R$  individually to the Yukawa couplings  $\tilde{Y}'_L{}^e$  and  $\tilde{Y}'_R{}^e$ . We observe that for the same set of parameter ranges, the lighter charged VL lepton mass ( $M_{E_2}$ ) can at most reach 1 TeV while the mass of the heavier state ( $M_{E_1}$ ) can not be lower than a TeV. In this regard, we should mention that while scanning over the mass ranges, we impose the direct search limit on  $M_{E_2} > 103$  GeV given by LEP [24]. Also to note that, as the plots indicate, the lightest vector-like lepton  $E_2$  is mostly right-handed, while the heavier one  $E_1$  is mostly left-handed. We note that  $M_{E_2}$  is most sensitive to parameters  $\tilde{Y}'_R{}^e$  and  $M_R$ , while  $M_{E_1}$  is most sensitive to parameters  $\tilde{Y}'_L{}^e$  and  $M_L$ .

In Fig. 3, we plot the dependences on the parameter space for the vector-like neutrino masses ( $M_{\nu_1}$  and  $M_{\nu_2}$ ). Here  $\nu_1$  is the lightest neutrino state and the DM candidate (the brown-colored graphs on the left) and the second vector-like lightest neutrino is  $\nu_2$  (the blue-colored contours on the right). The variation is shown only with the relevant parameters, namely, the bare mass terms  $M_L$  and  $M_R$  which tune the masses of these neutral VL lepton candidates and with the Yukawa couplings  $Y'_L{}^\nu$  and  $h'_R$  which control the DM annihilation cross section and set its relic density. In consequence to the parameter scanning, we now proceed to our analysis on DM sector and collider signatures.

### 3 Dark Matter

For the vector-like neutrino to be a viable candidate for dark matter, it must satisfy conditions of providing the right level of relic abundance from thermal dark matter production in the early universe. In addition, as the lack of any dark matter signals in either direct or indirect dark matter detection experiments confront our theoretical expectations, these must satisfy increasingly severe constraints from experiments. For the dark matter analysis, we extend the left-right model in [43] to include vector-like leptons using `FeynRules` [44] and extract the resulting file in `CalcHEP` [45] to implement the model into `micrOMEGAs` [46]. We use `micrOMEGAs` to calculate the relic density ( $\Omega_{DM}h^2$ ), the spin-independent cross section ( $\sigma^{SI}$ ), the annihilation cross section ( $\langle\sigma v\rangle$ ), and the neutrino and muon fluxes, which are the most constrained observables for our model. We analyze these in turn below.

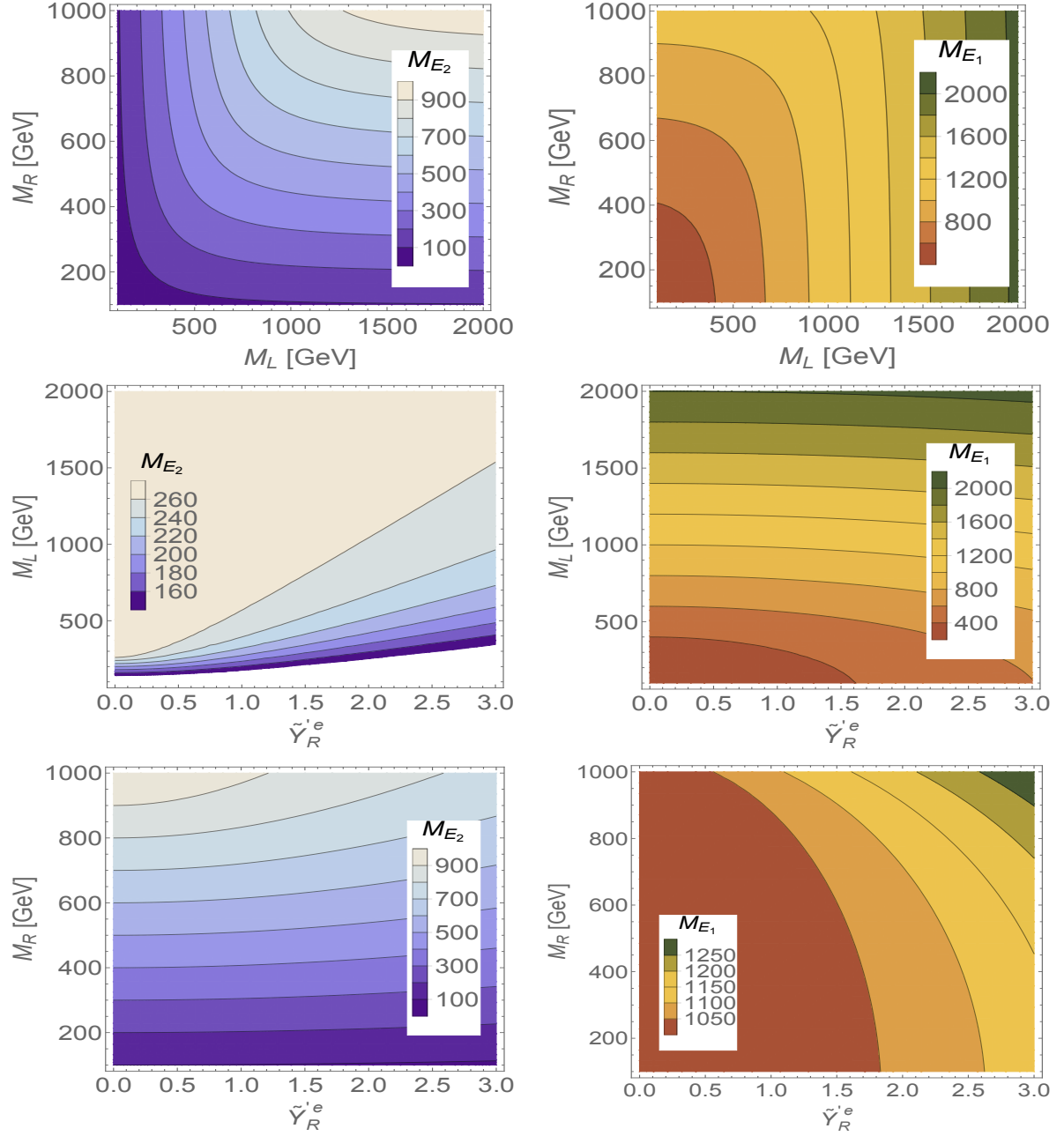


Figure 1: (Left panel) Contour plots showing the dependence of the lightest vector-like charged lepton masses ( $M_{E_2}$ ) on  $M_L, M_R$  for  $\tilde{Y}_R^e = 2.5$  (top); on  $M_L, \tilde{Y}_R^e$  for  $M_R = 275$  GeV (middle); and on  $M_R, \tilde{Y}_R^e$  for  $M_L = 1000$  GeV (bottom). (Right panel) Same contour graphs showing the dependence of the heavier vector-like charged lepton mass ( $M_{E_1}$ ). We take Yukawa couplings  $Y_L^e = 0.1, Y_R^e = 2.5$ . The panels on the right indicate the color-coded mass values for the contours.

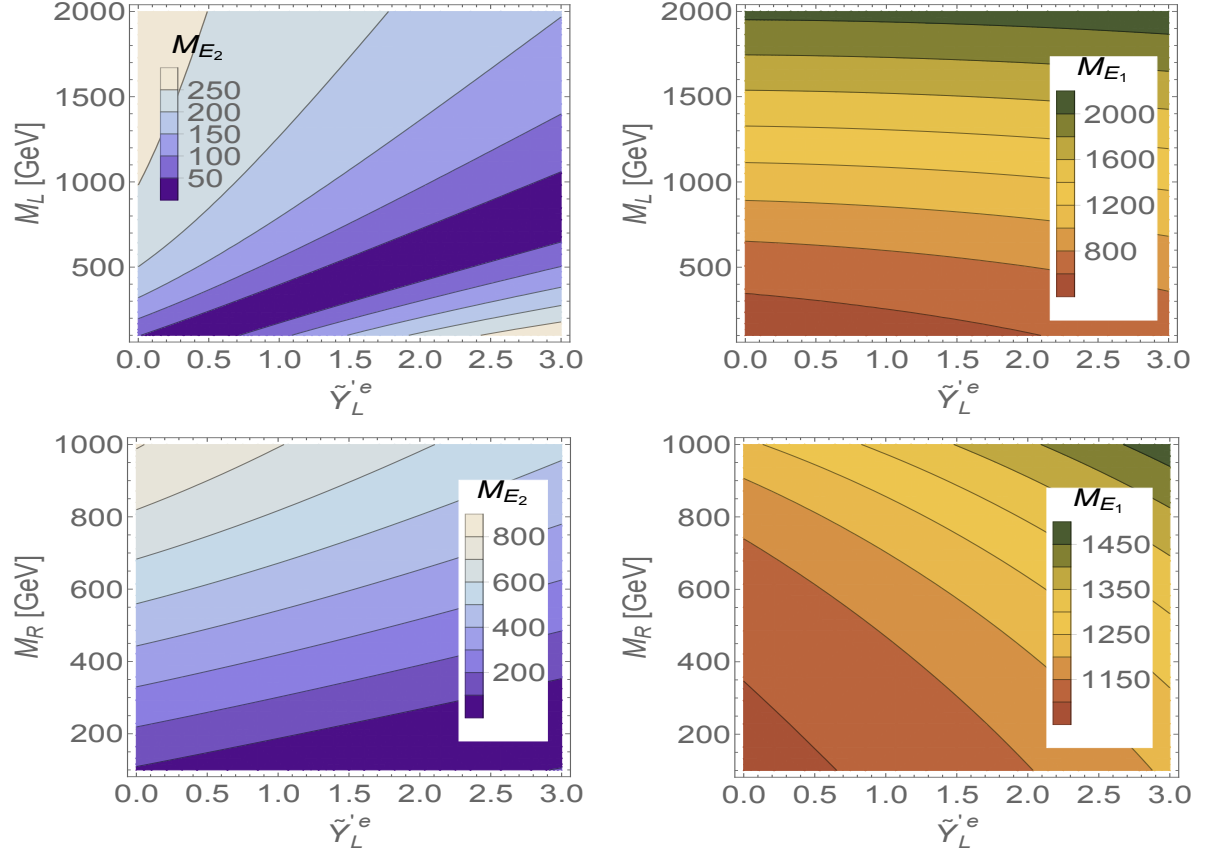


Figure 2: (Left panel) Contour plots showing the dependence of the lightest vector-like charged lepton masses ( $M_{E_2}$ ) on  $M_L, \tilde{Y}_L^e$  for  $M_R = 275$  GeV (top) and for  $M_R, \tilde{Y}_L^e$  for  $M_L = 1$  TeV (bottom). (Right panel) Same contour graphs, but for the heavier vector-like charged lepton mass ( $M_{E_1}$ ). As before,  $Y_L^e = 0.1, Y_R^e = 2.5$  and the panels on the right indicate the color-coded mass values for the contours.

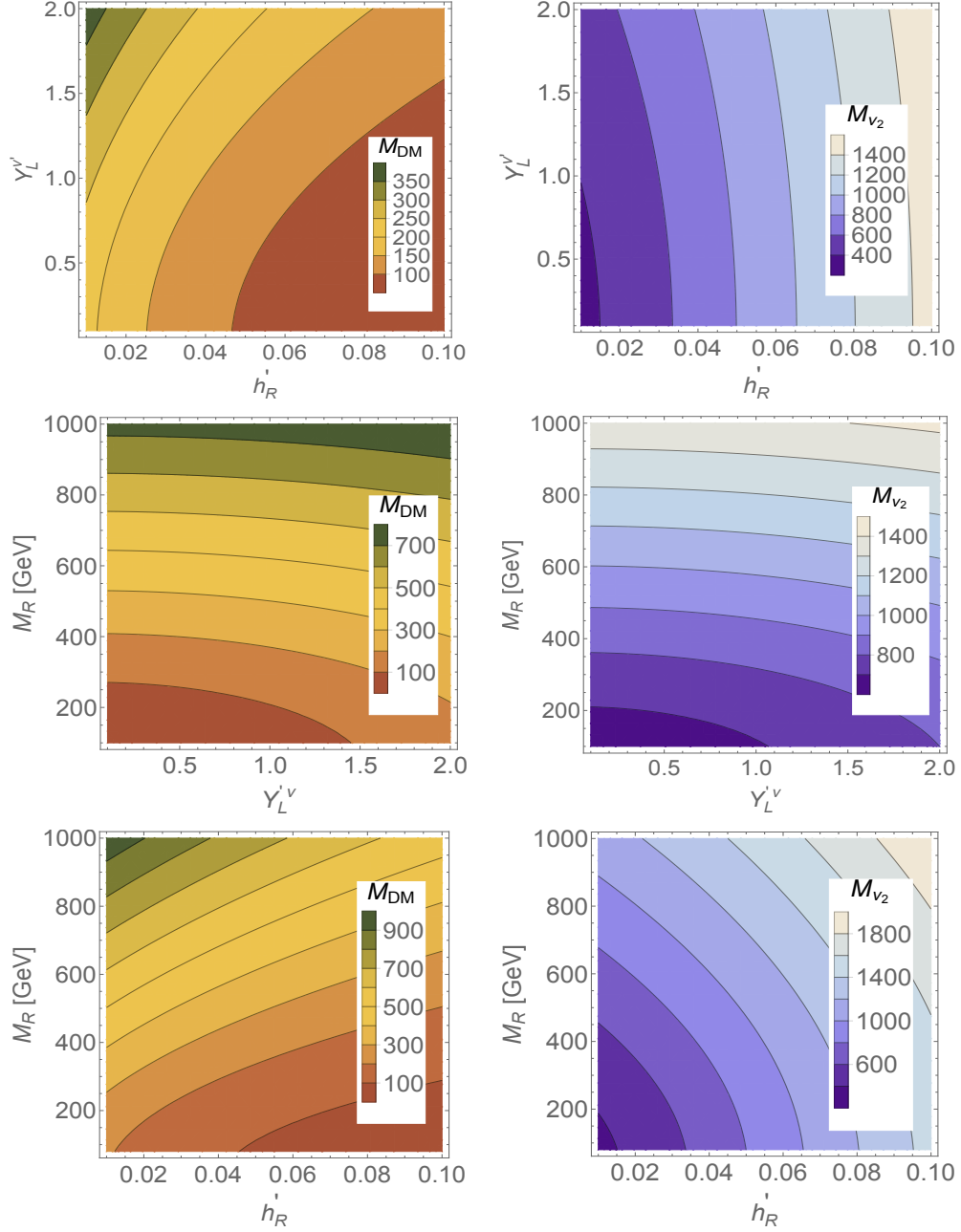


Figure 3: (Left panel) Contour graphs showing the dependence of the vector-like neutrino mass, for the lightest state  $\nu_1$  and (right panel) for the heavier state  $\nu_2$  as a function of  $Y_L^{\nu}$  and  $h_R$ , with  $M_R=275$  GeV (top), as a function of  $M_R$  and  $Y_L^{\nu}$  for  $h_R = 0.045$  (middle), and as a function of  $M_R$  and  $h_R$  for  $Y_L^{\nu} = 1.5$  (bottom). The panels on the right indicate the color-coded mass values for the contours.

### 3.0.1 Relic Density

First, we analyze the consequences of having the lightest vector-like neutrino as our dark matter candidate. Using the results in the previous sections, we explore the parameter space of the model which yields the correct relic density of dark matter, determined very precisely as the amount of non-baryonic dark matter in the energy-matter of the universe to be  $\Omega_{DM}h^2 = 0.1199 \pm 0.0027$  [47], with  $\Omega_{DM}$  the energy density of the dark matter with respect to the critical energy density of the universe, and  $h$  the reduced Hubble parameter.

For the purpose of comparing with the data, we include the  $2\sigma$  allowed range of relic density:  $0.1144 \leq \Omega_{DM}h^2 \leq 0.1252$ , as constrained by WMAP [48] and PLANCK [47]. The relic density depends on a number of parameters, but sensitively only on  $Y_L^{\nu'}$ ,  $M_R$  and  $h'_R$ . In Fig. 4 we present some contour plots to illustrate our parameter space. The contours indicate the points that respect the relic constraints for the given parameter space, and requiring  $M_{E_2} > 103$  GeV. The range of  $Y_L^{\nu'}$  is given in the color-coded column on the right, and we take throughout  $h'_R = 0.045$ . As the figure indicates, the range of parameters is restricted, but there are continuous values of  $M_{DM}$  which satisfy relic bounds for  $M_{E_2}$  in the range 250-1000 GeV.

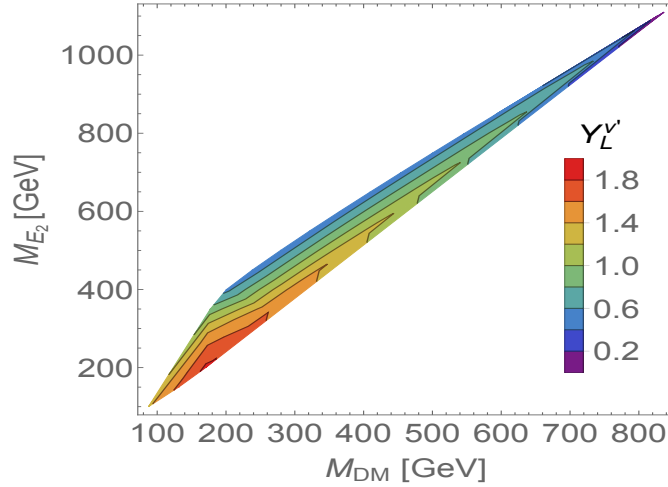


Figure 4: *Contour plots for the allowed relic density as a function of the vector-like lepton mass  $M_{E_2}$  and the vector-like neutrino (the dark matter candidate) mass (in GeV) for  $M_L = 1$  TeV. We impose the restriction  $0.1144 \leq \Omega_{DM}h^2 \leq 0.1252$ . The color code for the Yukawa coupling  $Y_L^{\nu'}$  is indicated on the right.*

### 3.0.2 Direct Detection

Direct detection experiments look for signals emerging from dark matter scattering off normal matter (neutrons or protons). As the dark matter only interacts weakly, such events are very rare, and direct detection experiments require very accurate background rejection. However, these are important, as the expected signals test the nature of the dark matter.

The interaction of dark matter with detector nuclear matter can be spin-dependent or spin-independent. The spin-dependent scattering can only happen with the odd number of the nucleon in the nucleus of the detector material, while in spin-independent (scalar) scattering, the coherent scattering of all the nucleons in the nucleus with the DM are added in phase. Consequently, in direct detection experiments, the experimental sensitivity to spin-independent (SI) scattering is much larger than to spin-dependent which experiences an enhancement in scattering from large target nuclei. In our case, the  $Z_L$ ,  $Z_R$  boson mediators influence the former, while Higgs bosons exchanges usually dominate the latter. The most stringent bounds on the spin-independent  $\sigma_{SI}$  cross section in terms of the dark matter mass come from the XENON100 [49] and LUX [50] experiments, which have seen no dark matter interaction events yet. We explore the spin-independent cross section and compare this against the constraints from XENON100 (dashed blue curve), the LUX experiment (dashed pink curve) and the projected XENON1T (dashed yellow curve) in Fig. 5, where, on the left, we plot the spin-independent dark matter cross section from direct searches as a function of the dark matter mass. As seen in the figure, the cross section predicted by our model (continuous red curve) mostly lies below the experimental bounds for  $M_{DM}$  values between 87.4 - 836.5 GeV (the exact region where we get the correct relic density), except in the region 70 - 150 GeV, where our theoretical expectations lie within the  $2\sigma$  expected sensitivity from XENON1T [51]. Increased precision may rule out lower dark matter regions of the parameter space. On the right, we plot the spin-dependent cross section, and the recent experimental limit from XENON100 [49]: the constraints imposed are much milder, and our cross section is smaller than the bound imposed by the data by 1-2 orders of magnitude.

### 3.0.3 Indirect Detection

Indirect detection experiments look for signals arising from pair annihilation of dark matter particles into SM particles. There are large number of final states that can be looked, including  $\mu^+$ ,  $\bar{d}$ ,  $\bar{p}$ ,  $\gamma$ -line and  $\gamma$ -continuum spectra. Since our dark matter candidate is primarily right-handed, the Higgs bosons (especially  $\Delta_R^0$ ), the  $Z_L$  and the  $Z_R$  can all act as mediators and enhance the dark matter-pair annihilation cross-section into fermion pairs. The coupling between the dark matter particle and SM mediators must produce an acceptable annihilation rate and, besides satisfying direct detection constraints, must be sufficient to produce correct relic density.

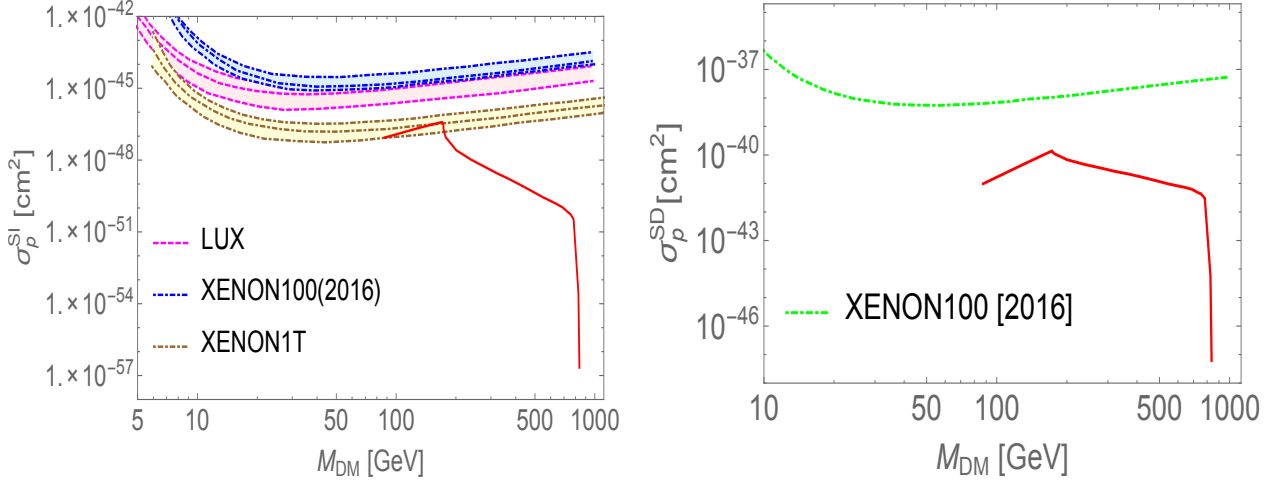


Figure 5: (Left) Spin-independent cross-section of the proton as a function of the dark matter mass in the left-right symmetric model with vector-like leptons (red curve), and the experimental upper limits from XENON100 [49] (dashed blue curve), from LUX [50] (dashed pink curve), and from XENON1T [51], all with  $2\sigma$  expected sensitivity (dashed yellow curve). (Right) Spin-dependent cross-section as a function of the dark matter mass (red curve) and the experimental limit from XENON100 [49]. We include only points in the parameter space where relic density constraints are satisfied.

The most stringent constraints on dark matter annihilation cross sections have been derived from the Fermi Gamma Ray Space telescope (Fermi-LAT) [52], used to search for dark matter annihilation products from dwarf spheroidal galaxies and the Galactic Center, which probe annihilation cross sections into photons. To obtain the correct value for the dark matter density the annihilation cross section should be  $\langle\sigma v\rangle \sim 3 \times 10^{-26} \text{cm}^3/\text{s}$ . In Fig. 6 we show the annihilation cross section of dark matter as a function of the dark matter mass  $M_{DM}$  and compare it with the constraints on the dark matter annihilation cross section for the most restrictive channels,  $\mu^+\mu^-$ ,  $b\bar{b}$  and especially  $W^+W^-$  channels, at 95% CL, found from examining continuum gamma-ray spectra from the dwarf spheroidal galaxy Segue I [52, 53]. Again, as seen in the figure, our parameter space survives limits from indirect detection, although in the region  $M_{DM} \in (175 - 300) \text{ GeV}$ , our theoretical prediction is close to the experimental limits.

The dark matter can annihilate into cosmic rays, over much different annihilation channels, for processes which are model dependent. Emission of most particles can be modeled by using leptonic equally well as hadronic scenarios. This ambiguity does not exist for high-energy neutrinos, as they can be created efficiently only in hadronic interactions via the decay of charged pions. The detection of a high-energy astrophysical neutrino source would then be a signal of accelerated hadrons. Each annihilation channel provides a unique neutrino energy spectrum and since the probability of neutrino detection depends sensitively on its energy, different neutrino signals can be expected from different annihilation channels. Also, since neutrinos interact only weakly with matter, they are insensitive



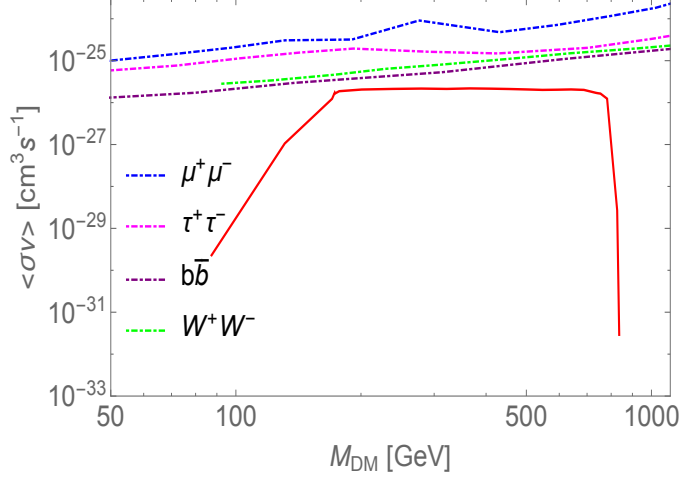


Figure 6: *Annihilation cross-section of dark matter into SM particles as a function of the dark matter mass (red curve). We compare with the combined indirect detection limits from Fermi-LAT and MAGIC collaboration on gamma rays arising from annihilations in dwarf spheroidal galaxies [53]. The dashed curves represent annihilation into  $\mu^+\mu^-$  (blue),  $\tau^+\tau^-$  (pink),  $b\bar{b}$  (purple) and  $W^+W^-$  (green). We include only points in the parameter space where relic density constraints are satisfied.*

to radiation fields and are accessible to cosmological distance scales. However, the same effect yields low cross-sections, and the backgrounds from existing atmospheric neutrinos is significant. For our vector-like neutrino dark matter candidate, annihilation in the galaxy into ordinary neutrinos  $\nu\bar{\nu}$  may be of significance. During propagation, neutrinos oscillate between flavors, but after traveling across cosmological distances, the coherence between different flavor states are lost and, as they reach Earth, neutrinos becomes mass eigenstates. These experiments also include limits on the muon flux, which incorporate limits for  $b\bar{b}$ ,  $\tau^+\tau^-$  and  $W^+W^-$  channels, for the purpose of comparing with other neutrino telescope experiments. In Fig. 7 we plot the flux as a function of the dark matter mass (neutrino flux in the left panel, muon in the right panel) and compare with the experimental limits from Baikal [54].

## 4 Collider Searches

In this section, we will analyze our findings in light of the collider searches for the new exotic vector-like leptons. As already explained in the previous section, the imposition of an extra parity symmetry provides a viable cold Dark Matter candidate. More explicitly, the lightest neutral vector-like lepton which is the lightest among the physical mass eigenstates defined in Eq. (23) acts as the good DM candidate. Also, the notable feature of the DM particle is that it is dominantly right-handed and thus can easily yield correct relic density within the  $2\sigma$  range of Planck’s latest relic density value  $\Omega_{DM}h^2 = 0.1199 \pm 0.0027$ , as we showed in Sec. 3. We have shown that there exists ample parameter

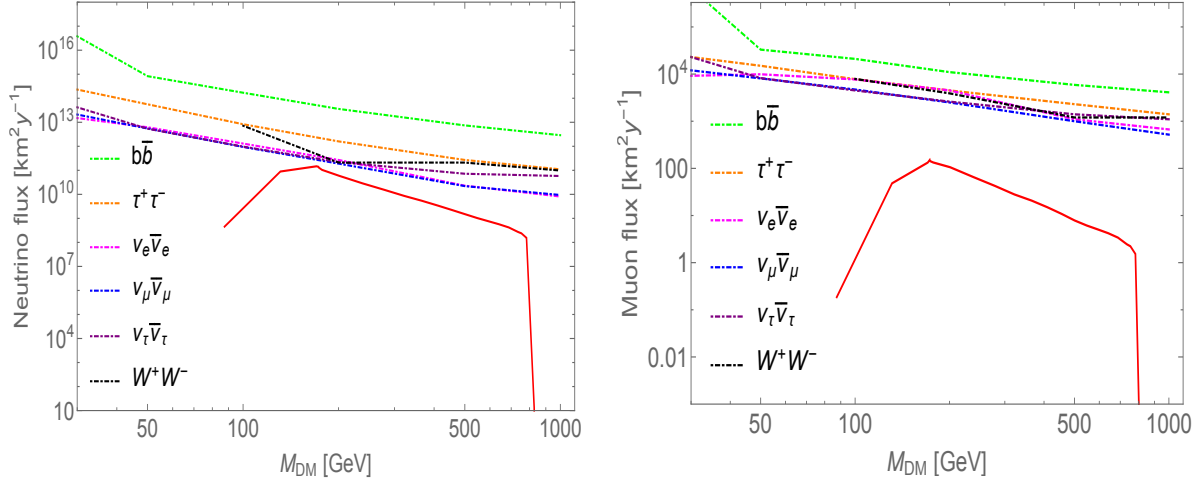


Figure 7: *Neutrino (left) and Muon (right) fluxes as a function of dark matter mass (red curve). The dashed curves represent 90 % CL upper limits from Baikal [54]. We include only points in the parameter space where relic density constraints are satisfied.*

space which satisfies all the DM constraints, including relic density and direct detection data. However, in addition to the DM vector-like neutrino, the model consists of extra charged vector-like (VL) leptons, which can decay into final states including DM. An obvious question would be to know if in the allowed parameter region, could there be any signature of these charged leptons in the existing or upcoming collider experiments.

#### 4.1 Benchmark Points

At this point, we would like to review our choice of benchmark points and explain their plausibility. The vector-like lepton sector of this model depends upon 14 parameters, among which 12 are the Yukawa couplings connecting the non-standard charged and neutral leptons ( $Y_L$ ,  $Y_R$ ,  $h_L$  and  $h_{R\pm}$ ) to the Higgs bosons and, the rest are the two bare mass terms ( $M_L$ , and  $M_R$ ) for vector-like leptons. We are interested in the region of parameter space where the DM constraints are satisfied and the VL charged leptons are kinematically accessible both to the LHC with  $\sqrt{s} = 14$  TeV and at the proposed  $e^+e^-$  international linear collider with  $\sqrt{s} = 1$  TeV. In view of these, we first fix most of the Yukawa couplings and we choose different masses for the VL leptons by varying the bare mass parameters,  $M_L$  and  $M_R$ . It can be noted that the dominant right-handed nature of the DM ( $\nu_1$ ) and the lighter charged VL lepton ( $E_2^\pm$ ) demand a relatively smaller  $M_R$  than  $M_L$ , for both to acquire masses of the order of few hundred GeV. With this procedure, for a particular choice of DM mass, we get the correct relic density and direct detection cross section by mainly tuning the Yukawa parameter  $h'_R$ . In Table 1, we display the values for the Yukawa coupling parameters of our choice, while in Table 2, we

give the masses of the lightest charged and neutral leptons and the corresponding relic density, and direct detection cross section, both spin dependent and spin-independent, for the three benchmark points of our interest.

Yukawa Parameters	$Y_L^{'e}$	$\tilde{Y}_L^{'e}$	$Y_R^{'e}$	$\tilde{Y}_R^{'e}$	$Y_L^{'\nu}$	$Y_R^{'\nu}$	$\tilde{Y}_L^{'\nu}$	$\tilde{Y}_R^{'\nu}$	$h_L'$	$h_L''$	$h_R''$
Value	0.1	0.0	0.0	2.5	1.5	0.04	0.1	0.1	0.8	0.7	0.0

Table 1: *Fixed parameters for all benchmark points.*

Benchmark Points	$h_R'$	$M_L$ (GeV)	$M_R$ (GeV)	$M_{\text{DM}}$ (GeV)	$M_{E_2^\pm}$ (GeV)	$\Omega_{\text{DM}} h^2$	$\sigma_{\text{SD}}$ (pb)	$\sigma_{\text{SI}}$ (pb)
BP1	0.045	1000	275	173	275	0.116	$1.3 \times 10^{-4}$	$2.55 \times 10^{-11}$
BP2	0.033	2000	350	258	350	0.112	$4.3 \times 10^{-5}$	$4.3 \times 10^{-12}$
BP3	0.032	2500	400	299	400	0.117	$3.1 \times 10^{-5}$	$2.42 \times 10^{-12}$

Table 2: *Benchmark points for vector-like leptons, including masses with corresponding DM relic density and direct detection cross section.*

#### 4.1.1 Higgs Signal Strength

In our model, the lightest CP-even scalar state resembles the 125 GeV Standard Model-like Higgs boson discovered at the LHC. Therefore, it is important to check the signal strengths for the production and decays of this Higgs state in this model relative to the current experimental data. Since the tree-level couplings of the lightest CP-even Higgs boson with all the Standard Model particles remain unchanged, we do not expect any deviations in the tree level decay channels of this Higgs boson from that of the Standard Model one. The gluon fusion production is not affected by leptons, but the loop induced decay modes of Higgs into the diphoton channel will get extra contributions from singly and doubly charged scalars and also from the exotic vector-like charged lepton loops. The new VL charged leptons are expected to contribute destructively (with respect to the dominant  $WW$  loop contribution), as the fermion loop comes with a negative sign, while the charged scalar loops may enhance or suppress the decay depending on the sign of the coupling of the charged scalars to the lightest CP-even Higgs boson. For brevity, we do not give the general expression for the Higgs to diphoton decay width, which can, however, be found in literature [55–58]. The test is done only for the charged lepton mass values chosen in the above-mentioned benchmark points while the singly and doubly charged scalar masses are chosen as 243 and 305 GeV, respectively, throughout the analysis. The implications of these charged scalars in our collider study will be mentioned later. The Higgs couplings to these nonstandard charged scalars and the VL leptons are fixed for all benchmark points since the Yukawa parameters are kept fixed. Moreover, there is no additional contribution to Higgs

production through gluon fusion, hence only the ratio of the partial decay width Higgs to diphoton channel between the model prediction to that of SM value represents our signal strength. According to the latest result from LHC Run II at 13 TeV, the Higgs to diphoton signal strength is  $0.85^{+0.22}_{-0.20}$  [59]. For our benchmark points, the signal strengths are, for BP1, BP2 and BP3, respectively, 0.59, 0.73 and 0.80, which are all within the  $2\sigma$  range of experimental data.

## 4.2 Searches at the LHC

In this section we consider the pair production of the lightest charged vector-like leptons, namely  $E_2^\pm$ , at the LHC.

$$p p \rightarrow E_2^+ E_2^-, \quad (24)$$

Instead of scanning over the multi-dimensional parameter space, we choose three benchmark points which are allowed by the constraints coming from the dark matter relic density and direct detection cross section.

In the chosen parameter region, these charged leptons can only decay to a SM  $W$  boson in conjunction with the DM particle ( $\nu_1$ ) with 100% branching fraction:  $E_2^\pm \rightarrow W^\pm \nu_1$ , thus leading to  $W^+ W^- + \cancel{E}_T$  final state, where  $\cancel{E}_T$  arises due to the presence of heavy neutral  $\nu_1$  particle, which is the cold dark matter candidate. Depending upon the decay mode of the Standard Model  $W$  boson, there are three possible final states :

$$\begin{aligned} (i) \quad & 2\ell^\pm + 0j + \cancel{E}_T, \text{ (both } W \text{ decay leptonically)} \\ (ii) \quad & 1\ell^\pm + 1j + \cancel{E}_T, \text{ (one } W \text{ decays leptonically, the other one decays hadronically)} \\ (iii) \quad & 0\ell^\pm + 2j + \cancel{E}_T, \text{ (both } W \text{ decay hadronically)}. \end{aligned} \quad (25)$$

where,  $\ell = e, \mu$ , and  $j$  corresponds to light quark jets. At this point, it should be mentioned that the final states closely resemble the pair production of SM  $W$ . However, in this case, one may expect to see some deviation in the shape of the  $\cancel{E}_T$  distribution compared to that of the SM  $W$ -pair signal. This change may be attributed to the fact that for the signal, the missing transverse energy comes from the massive neutral particle whereas in the SM background almost massless neutrinos are the decay products. Hence, we expect that the SM processes which contribute to the background for the SM  $W$ -pair signal will also play the same role in our signal process. Although the cross sections are higher for the final states (ii) and (iii), listed in Eq. (25), these final states are difficult to measure at the LHC because of the large background contributions mainly arising from  $t\bar{t}$ , single top,  $W^\pm + \text{jets}$  and other di-boson productions, all of which are difficult to suppress. Therefore, the di-leptons and

missing transverse energy ( $2\ell^\pm + \cancel{E}_T$ ) final state is the only possible channel to probe this vector-like heavy lepton signal at the LHC. As already mentioned, our signal process mimics the exact SM  $W$  pair production process but with different  $\cancel{E}_T$  spectrum. Hence, it is expected that the application of same event selection method for SM  $W$  pair production to our signal process will suppress the other dominant SM backgrounds to the final state (i). Therefore, to have an overview of signal significance, throughout our analysis, we only consider the SM  $W^+W^-$  process as the dominant background.

For our analysis, we supplement the model in [43] with VL leptons, using FeynRules [44] which gives the UFO model files required in Madgraph5 [60] to generate the signal events at the LO parton level. The SM background events are also generated using Madgraph5. The unweighted parton level events are passed through the Pythia(v6.4) [61] to simulate showering and hadronisation effects, including fragmentation. The Detector simulation is done using the Delphes(v3) [62]. Finally, we perform the cut analyses using MadAnalysis5 [63]. At this point, we would like to mention that at the detector level, the criteria for the isolation of electron and muon at the final state are performed using the method described in Ref. [64], where electrons are isolated with the **Tight** criterion defined in [65] and muons are isolated using the **Medium** criterion defined in [66]. Jets are reconstructed using the anti- $k_t$  clustering algorithm with radius parameter  $\Delta R = 0.4$  with minimum  $p_T = 20$  GeV and jets originating from the fragmentation of  $b$ -hadrons ( $b$ -jets), if any, are tagged with 85% tagging efficiency, and 10% and 1% mis-tagging efficiency for  $c$ -quark and light-quark jets respectively. The leading order (LO) production cross-sections are calculated using the NNPDF3.0 parton distributions. Before discussing the cut analyses, we show the histograms for the signal and background after imposing the basic cuts described previously.

In Fig. (8), we show the distribution of transverse momentum ( $p_T$ ) for the hardest (left panel) and second hardest (right panel) charged leptons in the event for the three benchmarks in Table 2. As expected, one may note that the signal and background distribution follows almost the same shape, including the visible Jacobian peak at half the  $W$  mass ( $m_W/2$ ), except for a little smearing effect mainly in the signal distribution for the highest  $p_T$  lepton, because in the signal case, the decaying  $W$  boson gets an extra inherent  $p_T$  from its parent vector-like charged lepton. Thus, it is important to note that we are not allowed to impose larger  $p_T$  cuts on the charged leptons than that applied in the SM  $W$  pair production case [64]. The deviation in the distributions of different benchmark points is self-explanatory from their different cross sections. In Fig. (9), we depict the distribution of the  $p_T$  of hardest jet and also the missing transverse energy  $\cancel{E}_T$  for all the three benchmark points. Analogous to the  $p_T$  distribution of hardest lepton, the hardest jet also shows a tail at the high  $p_T$  end. But since we have already chosen two lepton final states, the extra jets are only coming from the initial state radiation (ISR). The common kinematical feature of ISR jets [67] is a crucial dependence on the mass scale that is being probed at the collider experiment and usually the transverse momentum ( $p_T$ )

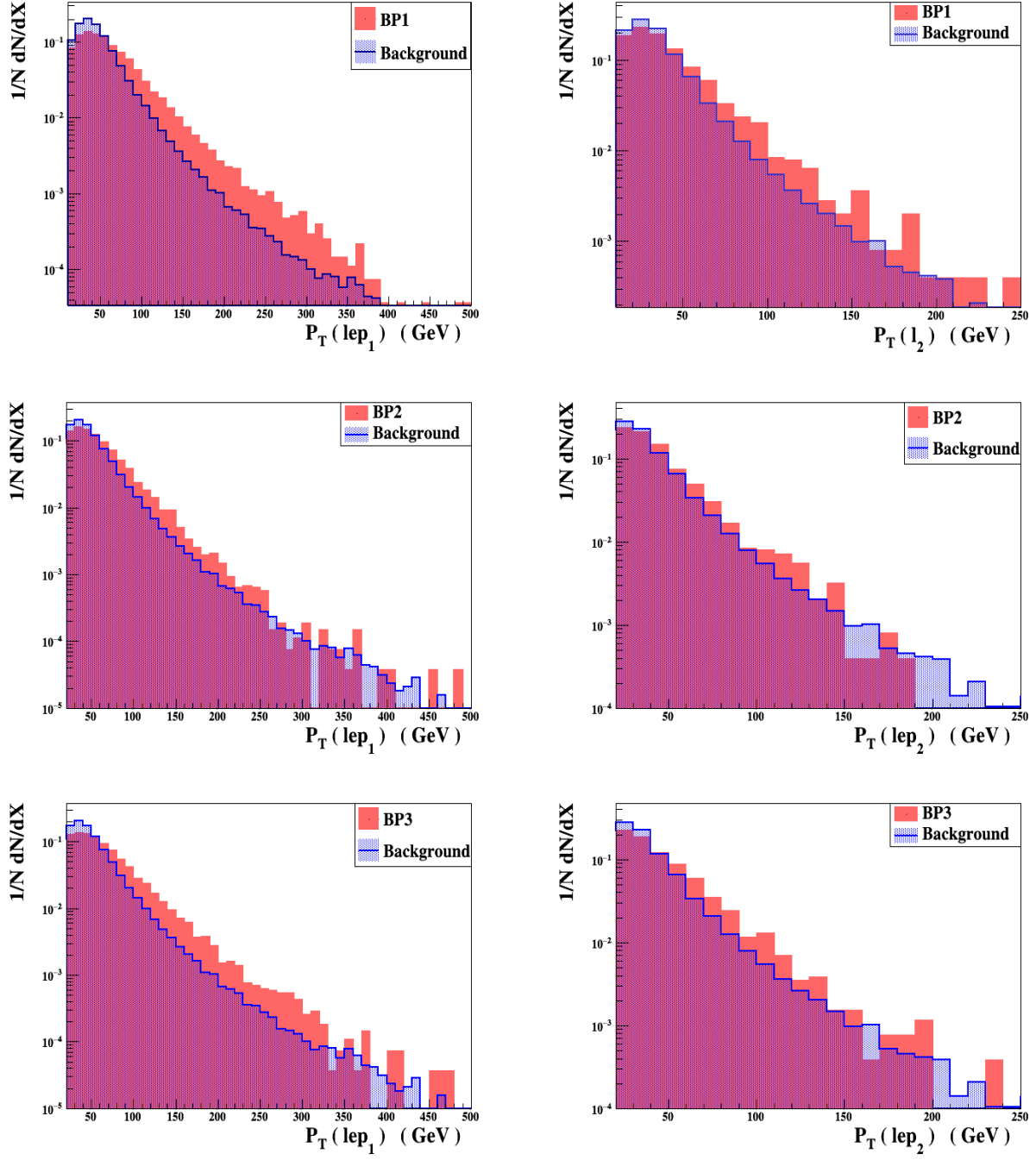


Figure 8: *Distribution for transverse momentum of hardest (left panel) and second hardest (right panel) lepton for three benchmark points, BP1, BP2 and BP3.*

of the ISR jets is higher with heavier BSM particles at the final state. Therefore, an upper cut on the  $p_T$  of any extra jets would yield a negative contribution to the signal significance for our final state, since the application of jet veto would be more stringent for the signal than the background. Note that the jet transverse momentum distribution, shown in Fig. 9, is obtained before applying any cuts and with inclusive decay modes of the  $W$  boson, and therefore the effect of ISR jets cannot be seen from here. On the other hand, the loss of significance can, however, be gained from the large  $\cancel{E}_T$  in the signal events. As already discussed, for the background events, the missing transverse energy arises only from the neutrinos or the mis-measurement of jets and photons, while, for the signal events, the lightest neutral VL lepton ( $\nu_1$ ) gives the dominant contribution to  $\cancel{E}_T$ , which is the stable DM candidate. The large mass range of this  $\nu_1$ , as shown in Table 2, as well as its inherently large  $p_T$  due to the mass difference between it and the decaying  $E_2^\pm$  significantly enhances the  $\cancel{E}_T$  for the signal events. Therefore, one can expect that demanding missing transverse energy  $\cancel{E}_T > 60$  GeV may help in suppressing the background and simultaneously improving the signal significance.

We now discuss the effect of selection cuts imposed over the basic cuts. It should be mentioned here that the analysis is done for LHC run at 14 TeV and the expected reach of integrated luminosity is  $3000 \text{ fb}^{-1}$ . Therefore, we seek to examine the maximum reach of signal significance at  $3000 \text{ fb}^{-1}$ , with the significance defined by

$$S = \frac{N_S}{\sqrt{N_S + N_B}}, \quad (26)$$

where  $N_S$  and  $N_B$  represent the number of signal and background events respectively.

Akin to the selection cuts imposed in Ref. [64], we list up the selection cuts that are imposed in our case in Table 3.

Cuts Name	Selection Criteria
C1	Number of Jets with $p_T(j) > 30$ GeV and $ \eta  < 4.5 = 0$
C2	At least two leptons with $p_T(\ell) > 25$ GeV
C3	Number of additional leptons with $p_T(\ell) > 10$ GeV = 0
C4	$\cancel{E}_T > 60$ GeV
C5	Number of b-tagged jets with $p_T(b) > 20$ GeV = 0

Table 3: *Selection Cut requirements.*

We then pass our simulated signal and background events through the cut selection and check the corresponding significance reach at the highest possible integrated luminosity that can be attained at the LHC. We sum up this in Table 4. As it can be seen from this Table that the maximum significance  $\sim 3\sigma$  is attained for the BP1, which has the largest production cross-section for the vector-like lepton pairs. For other two benchmarks, the signal significance is rather poor. From this analysis it is very

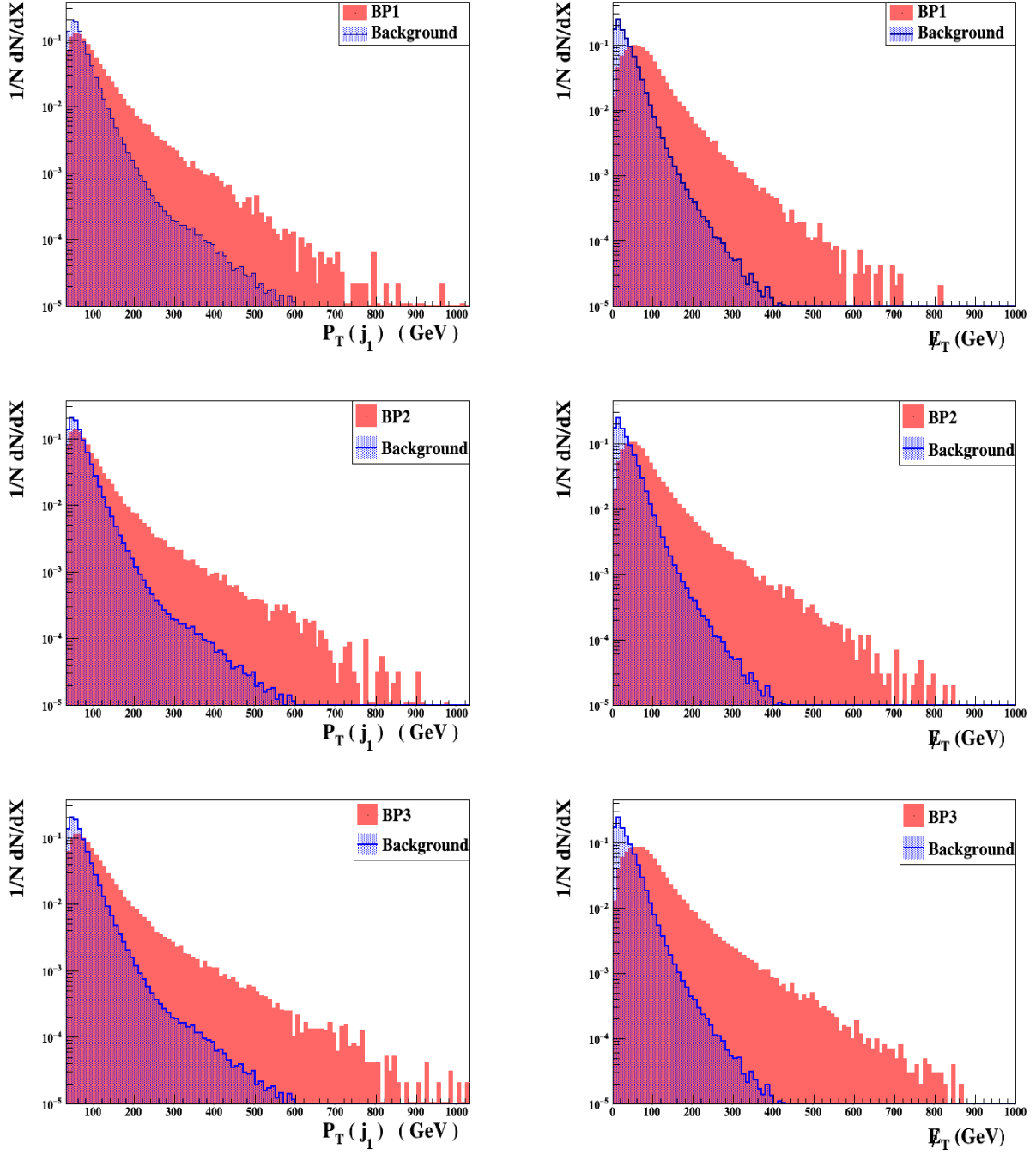


Figure 9: *Transverse momentum of hardest jet and missing transverse energy distribution for three benchmark points BP1, BP2 and BP3.*



clear that it would be extremely difficult to probe the vector-like leptons scenario at the 14 TeV LHC run even with the highest possible luminosity attainable at that energy. Thus we are motivated to look for the same signal process for the same benchmark points at the upcoming International  $e^+e^-$  Linear Collider (ILC) experiment.

	Production cross section ( $fb$ )	Effective cross sections in $fb$ after Cuts					Significance reach at $\mathcal{L}_{\text{int}} = 3000 fb^{-1}$
		C1	C2	C3	C4	C5	
SM Background	70940	6608	558.9	558.9	178.2	177.2	–
BP1	138.4	9.43	1.33	1.33	0.69	0.69	2.83
BP2	53	3.69	0.47	0.47	0.22	0.22	0.90
BP3	31	1.94	0.29	0.29	0.15	0.15	0.01

Table 4: *Effective cross section obtained after each cut for both background and signal and the respective significance reach at  $3000 fb^{-1}$  integrated luminosity at 14 TeV LHC.*

To conclude this subsection, we have shown that pair production of VL leptons is not very promising at the LHC, and would require very high luminosity to disentangle the signal from the background.

### 4.3 Searches at the ILC

In view of the fact that the plausible signal for probing the lightest charged VL leptons at the LHC seems difficult to observe, and requires much higher luminosity than that may be reached, we look for the possibility of probing the same signal at the upcoming International Linear Collider (ILC). The ILC is favored for its clean signal and less background noise, which at LHC originates mainly from the QCD processes. At the LHC, higher order perturbative QCD corrections as well as nonperturbative QCD effects give rise to large systematic uncertainties in theoretical calculations and hence precision measurements does not seem to be feasible. On the contrary, the initial state particles ( $e^-$  &  $e^+$ ) at the ILC are point-like elementary particles and only interact through electroweak interactions with only a few percent level modification in radiative corrections. This is why the ILC results provide better high precision and thus help theoretical understanding of Standard Model signal and background processes, which may also shed some light on the presence of subtle new physics interactions. In addition to this, the ILC will also be furnished with polarized electron and positron beams so that the processes can be completely characterized based on each initial and final polarization state. For the signal process, we consider exclusive leptonic final states and hence a better significance than at the LHC is naturally expected. In the following subsection, we perform the analysis for the pair production of the lightest charged VL leptons, namely,  $E_2^\pm$ , at the ILC. Equivalent to Eq. (24), the process of interest in this

case is

$$e^+ e^- \rightarrow E_2^+ E_2^- . \quad (27)$$

To compare with our previous result on the searches at the LHC, here we also consider only the di-lepton final state, as mentioned in (i) of Eq. (25)<sup>9</sup>. In addition to this, we also perform the analysis of VL leptons production using some particular choice of polarization for the incoming electron and positron beams. Explicitly, we consider three distinct combinations [69],

- (a) Both electron and positron beams are unpolarized.
- (b) Electron beam is 80% left-polarized and positron beam is 60% right-polarized.
- (c) Electron beam is 80% right-polarized and positron beam is unpolarized.

For an extensive review on the physics case for the polarized beam at the ILC, we refer to [70]. In Fig. 10, we show the production cross section for our process, given in Eq. (27), at the ILC center of mass energy 1 TeV. We indicate our chosen benchmark points on the graphs. It is to be noticed that the polarization states of the initial electron and/or positron beams change the signal cross section significantly. The highest production cross section can be reached for the combination (b), defined previously. The collider analysis is done using **Madgraph5**. In compliance with LHC searches, here too the dominant SM background for di-lepton final states is SM W-boson pair production.  $WWZ$  and  $ZZ$  will also contribute to background, *albeit* with small cross-sections.

Before imposing selection cuts, we check the distributions of various kinematical variables at the parton level. To do so, some basic cuts are enforced first, such as,

- the minimum transverse momentum of the charged lepton at the final state should be greater than 10 GeV ( $p_{T\ell} > 10$  GeV), and
- the pseudo-rapidity of each charged lepton must be within 2.5 ( $|\eta_\ell| < 2.5$ ).

In Fig. 11, the transverse momentum ( $p_T$ ) and pseudo-rapidity ( $\eta$ ) distribution for the hardest lepton in the final state is shown for all the three polarization combinations. The same is shown in Fig. 12, but for the second hardest lepton. We mention here that as an example plot, we only show the distributions for our first benchmark point (BP1), which is the most promising for the experimental detection of our chosen process.

---

<sup>9</sup>A similar study on VL charged lepton search at the ILC is done in [68].

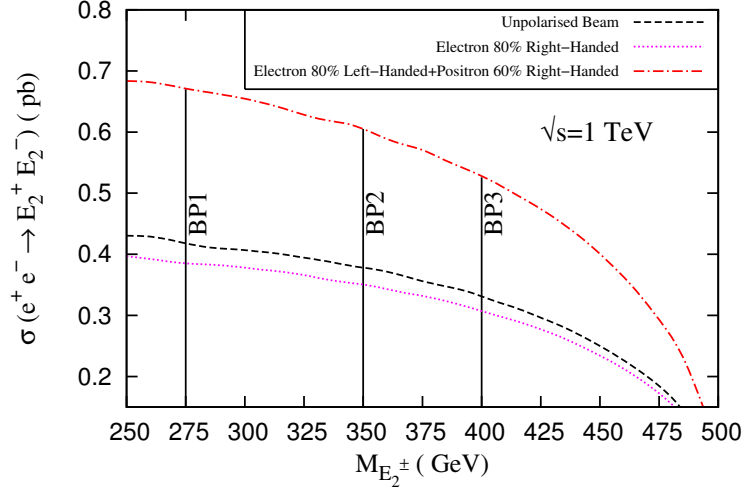


Figure 10: *Signal cross-section for different polarization states of incoming electron and positron beam at the ILC for various VL charged lepton masses.*

The point to be noted here is that for all the cases, the lepton  $p_T$  spectrum for the SM background is relatively harder than that of the signal distribution. This feature can be understood from the fact that for SM background, leptons originate from the direct production  $W^\pm$  bosons whereas in the signal process they come from the cascade decay of heavy leptons  $E_2^\pm$ . This also explains why the pseudo-rapidity distribution of the leptons is mostly central for the signal, unlike the  $WW$  and  $ZZ$  case where leptons show peaking behaviour at large pseudo-rapidities. However, due to the 3 body kinematics of the  $WWZ$  process, the pseudo-rapidity distribution of leptons coming from this process are evenly distributed over the full rapidity range  $(-2 \text{ to } +2)$ . Keeping this in mind, one can also similarly interpret the distribution of  $\Delta R$  between the two leptons, which we show in Fig. 13, where  $\Delta R$  is defined as the measure of angular separation between the two charged leptons by means of their difference in pseudo-rapidity ( $\eta$ ) and azimuthal angle ( $\phi$ ):  $\Delta R = \sqrt{(\Delta\eta)^2 + (\Delta\phi)^2}$ . Both of the charged leptons are generated from one single  $Z$  boson for  $ZZ$  background and therefore the separation is less than the signal and  $WW$  background, where the leptons come from two  $W$ 's with large angular separation.

At this point, it is worth mentioning that the di-lepton final state may also arise from pair production of the singly charged scalar states. The charged Higgs masses only depend on the scalar quartic coupling of Eq. (16) and are independent of the parameter space that we chose for our benchmark points in VL lepton searches. But the production cross section times the branching ratio to di-lepton final states is much lower than that we get from  $E_2$  pair production, and so it contributes negligibly

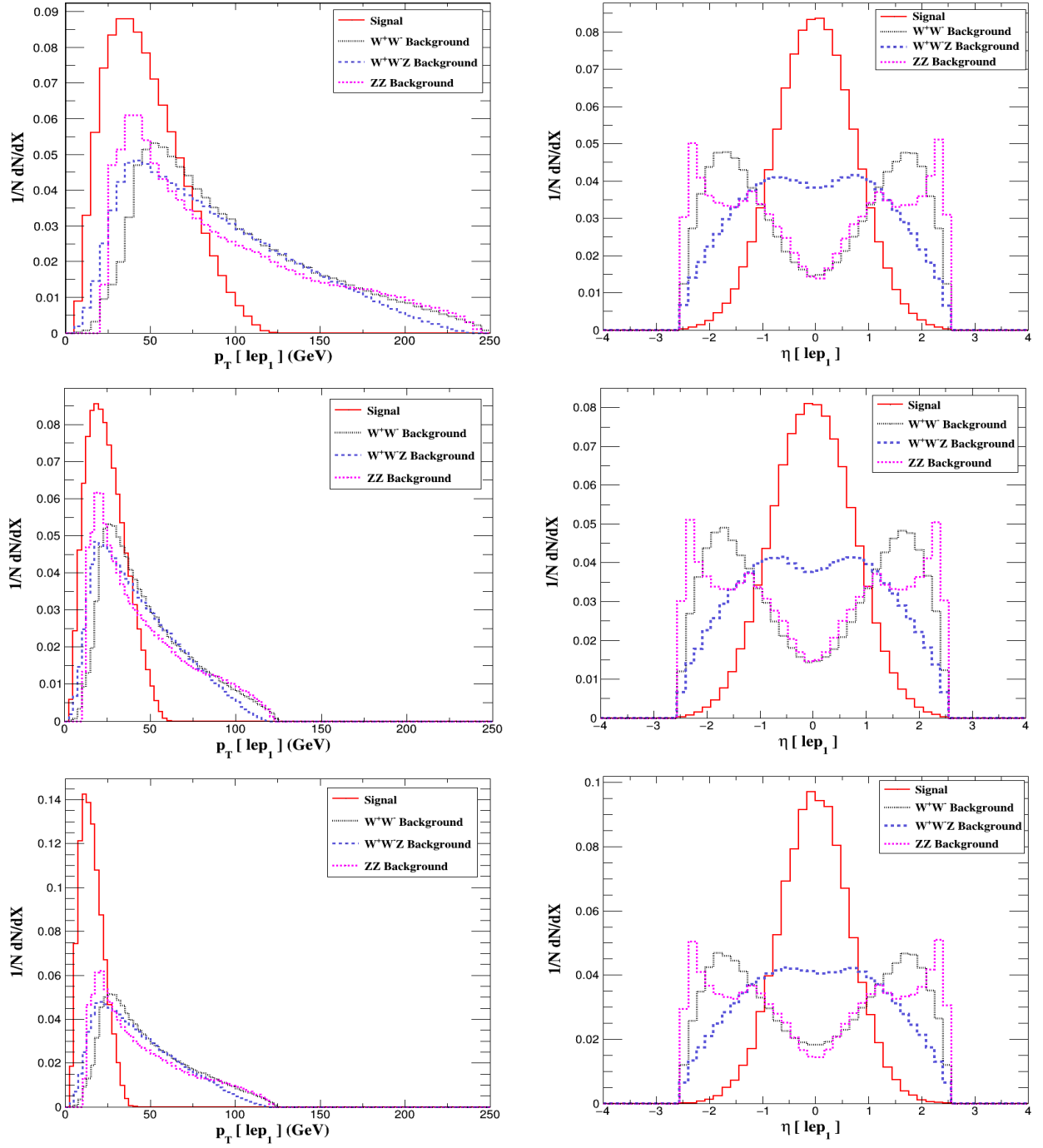


Figure 11: *Transverse momentum and pseudo-rapidity distribution of the hardest lepton for BP1 and for combination (a) unpolarized (top), (b) both-polarized (middle) and (c) only electron-polarized(bottom) respectively.*

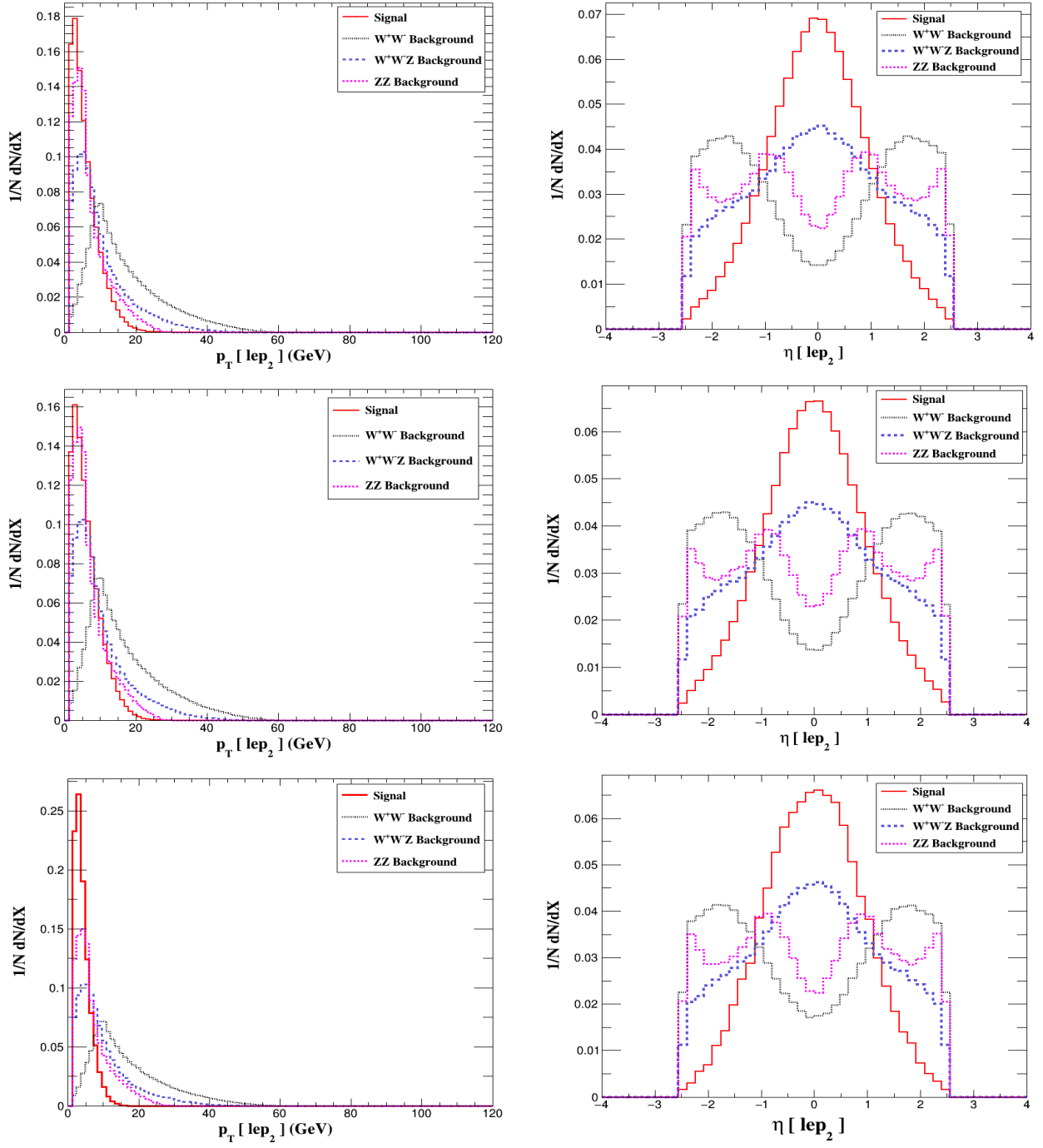


Figure 12: *Transverse momentum and pseudo-rapidity distribution of the second hardest lepton for BP1 and for combination (a) unpolarized (top), (b) both-polarized (middle) and (c) only electron-polarized (bottom) respectively.*

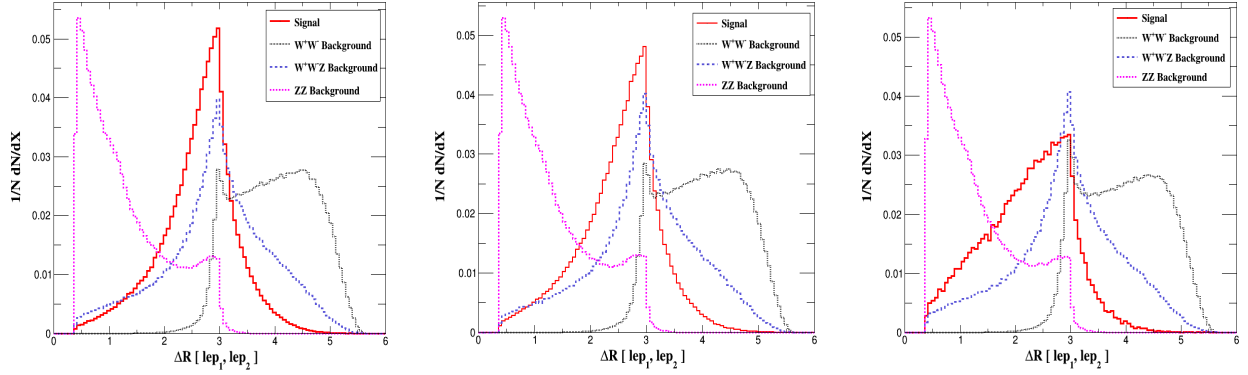


Figure 13:  $\Delta R$  distribution of the two leptons for BP1 and for combination (a) unpolarized (left), (b) both-polarized (middle) and (c) only electron-polarized (right) respectively.

to final significance<sup>10</sup>. In this respect, it should also be mentioned that the same recipe also applies to our studies for the LHC searches but similar to this case, the effective cross section for pair-production of singly charged scalar decaying to di-lepton final states at LHC is too small to add anything to the final signal significance<sup>11</sup>.

Investigating the distributions of the above-mentioned kinematic variables, we choose our final selection cuts. First of all, from Fig. 13 one can see a significant deviation in the spectrum of  $\Delta R(\ell_1, \ell_2)$  between our signal and the SM background, mainly from  $ZZ$  and  $WWZ$  processes. We thus select events with di-leptons, where the angular separation between the two leptons must satisfy our first selection cut,  $2 < \Delta R(\ell_1, \ell_2) < 3.5$ . Next, following the distributions in Fig. 11, we see that a choice of the hardest lepton  $p_T$  between 25 GeV to 160 GeV along with pseudo-rapidity within central region ( $|\eta(\ell_1)| < 1.5$ ) may enhance the signal significance by considerably reducing the main  $WW$  background. However, one should know that these additional cuts are chosen by only analyzing the unpolarized scenario and kept same for two other polarization combinations. Modification of selection cuts according to specific polarization cases will further increase our final signal significance. The last selection cut on the transverse momentum and pseudo-rapidity of the second hardest lepton follows the same logic as of the selection cut on hardest lepton. All the selection cuts are displayed in Table 5.

Cuts Name	Selection Criteria
C1	$2 < \Delta R(\ell_1, \ell_2) < 3.5$
C2	At least one lepton with $25 < p_T(\ell_1) < 160$ GeV and $ \eta(\ell_1)  < 1.5$
C3	At least two leptons with $p_T(\ell_2) > 20$ GeV $ \eta(\ell_2)  < 1.5$

Table 5: The cuts implemented for ILC search.

<sup>10</sup>The scalar sector of this model can, however, be detected from other interesting final states but this is beyond the scope of this work and will be addressed in a future project.

<sup>11</sup>A study on the heavier state of the scalar sector of the model at the High Energetic Future Hadron Collider can be found in [38].

		Effective Cross-section (fb) after the cut			$\mathcal{L}_{5\sigma}$ ( $fb^{-1}$ )
SM-background	Production Cross-sec. (fb)	C1	C2	C3	
$W^+ W^-$	56.5	12.62	1.36	1.16	
$W^+ W^- Z$	0.44	0.21	0.057	0.037	
$Z Z$	2.13	0.46	0	0	
Total background				1.197	
BP1	17	12.31	10.4	8.81	3.22
BP2	14.5	9.44	9.02	7.45	3.89
BP3	12.8	7.68	7.33	5.85	5.16

Table 6: *Effective cross sections after each cut for both background and signal, and the integrated luminosity required for  $5\sigma$  significance ( $\mathcal{L}_{5\sigma}$ ) at 1 TeV ILC for unpolarized incoming beam.*

The cut-flow and the required integrated luminosity for  $5\sigma$  discovery reach are given in Table 6, Table 7 and in Table 8 respectively for polarization combinations (a), (b) and (c), i.e. for completely unpolarized initial states, both electron (80%left) and positron (60%right) beams are polarized and only right-polarized electron (80%) beam. The significance is calculated using the same relation given in Eq. (26).

		Effective Cross-section(fb) after the cut			$\mathcal{L}_{5\sigma}$ ( $fb^{-1}$ )
SM-background	Production Cross-sec. (fb)	C1	C2	C3	
$W^+ W^-$	162	35.75	3.93	3.35	
$W^+ W^- Z$	1.2	0.64	0.17	0.11	
$Z Z$	4.4	1.0	0	0	
Total background				3.46	
BP1	27.7	20.58	17.13	14.76	2.09
BP2	23.5	16.1	15.52	13.02	2.44
BP3	20.64	12.89	12.39	10	3.37

Table 7: *Effective cross sections after each cut for both background and signal, and the integrated luminosity required for  $5\sigma$  significance ( $\mathcal{L}_{5\sigma}$ ) at 1 TeV ILC for both polarized incoming beam.*

Let us understand the aftermath of selection cuts for all the three cases. As expected, the  $\Delta R$  selection cut (C1) seems quite competent in suppressing mainly the SM background. While almost 75% signal events pass the cut, only 22% of  $WW$  background events remain unaffected. The signal significance is

better when the other two cuts (C2) and (C3) are applied on top of (C1). Quantitatively, almost 90% background events fail to overcome Cut 2 (C2) selection barrier while around 85% of signal events survive. The last cut (C3), however, may not play a convincing role in enhancing the signal significance, but the requirement of a second lepton is mandatory to avoid other unwanted SM backgrounds.

		Effective Cross-section(fb) after the cut			$\mathcal{L}_{5\sigma}$ ( $fb^{-1}$ )
SM-background	Production Cross-sec. (fb)	C1	C2	C3	
$W^+ W^-$	11.7	2.89	0.31	0.27	
$W^+ W^- Z$	0.09	0	0	0	
$Z Z$	1.4	0.32	0	0	
Total background				0.27	
BP1	15.62	10.99	9.45	7.86	3.29
BP2	13.4	8.3	7.83	6.37	4.08
BP3	11.9	6.85	6.5	5.11	5.16

Table 8: *Effective cross sections after each cut for both background and signal and the integrated luminosity required for  $5\sigma$  significance ( $\mathcal{L}_{5\sigma}$ ) at 1 TeV ILC for only electron beam polarized.*

Reviewing the cut-flow tables, we observe that the required integrated luminosity for a  $5\sigma$  discovery reach is quite low, about  $2\text{-}5\text{ }fb^{-1}$ , which can easily be reached even in the first run of the ILC. The best possible channel turns out to be the benchmark point BP1, with both the initial electron and positron beams polarized as 80% left and 60% right helicity states, and where the required integrated luminosity for discovery reach is as low as  $2.09\text{ }fb^{-1}$ . All the rest of the benchmarks and beam polarization states are also promising and can easily be tested at the upcoming ILC searches.

Over all, we see that the VL charged leptons have a clearer signature at the ILC than that at the LHC where they are extremely difficult to probe, even with the highest possible reach of integrated luminosity.

## 5 Conclusion

We present a complete and thorough investigation of the effects of introducing vector-like leptons into left-right symmetric models. Our aim is to adjoin one missing piece, a dark matter candidate, into the model. In keeping with the symmetries of the model, two vector-like doublets are introduced, one left-handed and one right-handed, together with their mirrors. A discrete parity symmetry forbids



mixing of vector-like particles with ordinary leptons: this is introduced for simplicity, as mixing can occur, but, given constraints from flavor-changing decays such as  $\mu \rightarrow e\gamma$ , only with the third family, and even there the mixing is constrained to be small as not to spoil low energy phenomenology results.

However, in the absence of mixing with SM leptons, the vector-like leptons mix among themselves and the lightest state (electrically neutral, and mostly right-handed) is stable and can serve as dark matter candidate. We show that, for a large range of the parameter space, this vector-like neutrino obeys constraints from the relic density abundance. In direct detection, the limits on spin-dependent cross sections do not restrict the parameter space, while the spin-independent cross section falls below the LUX and XENON100 limits, whereas XENON1T puts pressure on the lighter (70-150 GeV) region of dark matter mass, which lies within its  $2\sigma$  sensitivity curves, rather than below. For indirect detection, we analyze the annihilation cross section into SM particles and show that it is safely below the Fermi-LAT limits, and the muon and neutrino fluxes coming from cosmic rays, also agree with experimental bounds from neutrino telescopes.

Finally, we investigate the distinctive signals of this scenario at colliders. At the LHC, the pair production of the lightest vector-like charged leptons, each decaying further into a  $W$  boson and dark matter yielding  $W^+W^- + \cancel{E}_T$ , is analyzed and compared to the background coming from SM  $W$  pair production. We devise three benchmarks obeying all dark matter and Higgs signal constraints, and show that, with judicious background cuts and at HL (high luminosity) LHC, one benchmark could reach  $\sim 3\sigma$  signal to background significance. At this point, we advocate the idea of testing our model at upcoming electron-positron collider experiment (ILC), in particular for our search channel. The ILC experiment is generally preferred over the hadron colliders because of its clean environment and ability to provide high precision measurements. Here, we mainly opt for the ILC because of its two main special characteristics. Firstly, the final state with VL charged leptons can be easily probed with much less SM background interference and secondly, ILC provides us with its distinct feature of polarized incoming electron and positron beams, which makes the search channel easier to investigate. In particular, we consider three distinct combinations of beam polarizations, named (a), (b), (c), respectively, for the cases where both incoming beams are unpolarized, the electron beam is 80% right-polarized and positron beam is 60% right-polarized and finally where only the electron beam is 80% right-polarized with completely unpolarized positron beam. Since, our signal resembles mostly SM  $W$  pair production, the enhancement (suppression) in production cross-section with incoming beam polarization follows the same rule as SM  $WW$  background does. Similar as for the LHC scenario, we illustrate our search strategies using the same benchmark points as before. The dominant background here is also the SM  $W^+W^-$  pair production, with small contributions from  $W^+W^-Z$  and  $ZZ$ . The most convenient kinematic variables to distinguish the signal from background is the pseudo-rapidity of the two charged leptons in the final state and specifically the angular separation ( $\Delta R$ ) between

them. With strategic cuts on these variable lead to large signal significance for the pair production of vector-like leptons. Moreover, the choice of polarized beam combination (*b*), where the electron beam is 80% left polarized and positron beam 60% right polarized, renders the best possible signal significance. A  $5\sigma$  discovery reach, in this case, can easily be attained even with integrated luminosity as small as  $2 \text{ fb}^{-1}$  for the highest production cross section benchmark BP1. The other polarization combinations are also impressive and can be tested even at the very first run of the ILC.

Our analysis strategy demonstrates the viability of the model prediction both for DM detection and collider signatures at the upcoming ILC. Our left-right model with dark matter is thus quite predictable and easily testable, perhaps at HL-LHC, and certainly at ILC.

## 6 Acknowledgments

MF thanks NSERC for partial financial support under grant number SAP105354. N.G. would like to thank the Council of Scientific and Industrial Research (CSIR), Government of India for financial support.

## 7 Appendix: eigenvalues for the vector-like neutrino mass matrix

We list the eigenvectors of the vector-like neutrino mass matrix Eq. 20.

$$\begin{aligned}
|\nu_1\rangle &\simeq \frac{M_{\nu_1} m'_\nu}{\sqrt{M_{\nu_1}^2 (M_R^2 + M_{\nu_1}^2) + m_\nu'^2 (M_L^2 + M_{\nu_1}^2)}} |\nu'_L\rangle + \frac{M_{\nu_1}^2}{\sqrt{M_{\nu_1}^2 (M_R^2 + M_{\nu_1}^2) + m_\nu'^2 (M_L^2 + M_{\nu_1}^2)}} |\nu_R'^c\rangle \\
&+ \frac{M_L m'_\nu}{\sqrt{M_{\nu_1}^2 (M_R^2 + M_{\nu_1}^2) + m_\nu'^2 (M_L^2 + M_{\nu_1}^2)}} |\nu_R''^c\rangle + \frac{M_R M_{\nu_1}}{\sqrt{M_{\nu_1}^2 (M_R^2 + M_{\nu_1}^2) + m_\nu'^2 (M_L^2 + M_{\nu_1}^2)}} |\nu_L''\rangle \\
|\nu_2\rangle &\simeq \frac{M_{\nu_2} m'_\nu}{\sqrt{M_{\nu_2}^2 (M_R^2 + M_{\nu_2}^2) + m_\nu'^2 (M_L^2 + M_{\nu_2}^2)}} |\nu'_L\rangle + \frac{M_{\nu_2}^2}{\sqrt{M_{\nu_2}^2 (M_R^2 + M_{\nu_2}^2) + m_\nu'^2 (M_L^2 + M_{\nu_2}^2)}} |\nu_R'^c\rangle \\
&+ \frac{M_L m'_\nu}{\sqrt{M_{\nu_2}^2 (M_R^2 + M_{\nu_2}^2) + m_\nu'^2 (M_L^2 + M_{\nu_2}^2)}} |\nu_R''^c\rangle + \frac{M_R M_{\nu_2}}{\sqrt{M_{\nu_2}^2 (M_R^2 + M_{\nu_2}^2) + m_\nu'^2 (M_L^2 + M_{\nu_2}^2)}} |\nu_L''\rangle \\
|\nu_3\rangle &= \frac{1}{\sqrt{2}} (|\nu'_L\rangle + |\nu_R''^c\rangle) \\
|\nu_4\rangle &= \frac{1}{\sqrt{2}} (|\nu'_L\rangle - |\nu_R''^c\rangle)
\end{aligned} \tag{28}$$

## References

- [1] R. N. Mohapatra and J. C. Pati, *A Natural Left-Right Symmetry*, *Phys. Rev.* **D11** (1975) 2558.
- [2] G. Senjanovic and R. N. Mohapatra, *Exact Left-Right Symmetry and Spontaneous Violation of Parity*, *Phys. Rev.* **D12** (1975) 1502.
- [3] R. N. Mohapatra and G. Senjanovic, *Neutrino Masses and Mixings in Gauge Models with Spontaneous Parity Violation*, *Phys. Rev.* **D23** (1981) 165.
- [4] C. Arbelez, M. Hirsch, M. Malinsk and J. C. Romo, *LHC-scale left-right symmetry and unification*, *Phys. Rev.* **D89** (2014) 035002, [[1311.3228](#)].
- [5] W.-l. Guo, L.-m. Wang, Y.-l. Wu and C. Zhuang, *The Dark Matter Constraints on the Left-Right Symmetric Model with  $Z(2)$  Symmetry*, *Phys. Rev.* **D78** (2008) 035015, [[0805.0401](#)].
- [6] W.-L. Guo, L.-M. Wang, Y.-L. Wu, Y.-F. Zhou and C. Zhuang, *Gauge-singlet dark matter in a left-right symmetric model with spontaneous CP violation*, *Phys. Rev.* **D79** (2009) 055015, [[0811.2556](#)].
- [7] W.-L. Guo, Y.-L. Wu and Y.-F. Zhou, *Exploration of decaying dark matter in a left-right symmetric model*, *Phys. Rev.* **D81** (2010) 075014, [[1001.0307](#)].
- [8] E. Ma, *Dark-Matter Fermion from Left-Right Symmetry*, *Phys. Rev.* **D85** (2012) 091701, [[1202.5828](#)].
- [9] P.-H. Gu, *A Left-Right Symmetric Model for Neutrino Masses, Baryon Asymmetry and Dark Matter*, *Phys. Rev.* **D81** (2010) 095002, [[1001.1341](#)].
- [10] M. Nemevsek, G. Senjanovic and Y. Zhang, *Warm Dark Matter in Low Scale Left-Right Theory*, *JCAP* **1207** (2012) 006, [[1205.0844](#)].
- [11] ATLAS collaboration, G. Aad et al., *Search for high-mass diboson resonances with boson-tagged jets in proton-proton collisions at  $\sqrt{s} = 8$  TeV with the ATLAS detector*, *JHEP* **12** (2015) 055, [[1506.00962](#)].
- [12] CMS collaboration, V. Khachatryan et al., *Search for heavy neutrinos and W bosons with right-handed couplings in proton-proton collisions at  $\sqrt{s} = 8$  TeV*, *Eur. Phys. J.* **C74** (2014) 3149, [[1407.3683](#)].
- [13] ATLAS collaboration, M. Aaboud et al., *Search for resonances in diphoton events at  $\sqrt{s}=13$  TeV with the ATLAS detector*, *JHEP* **09** (2016) 001, [[1606.03833](#)].

- [14] CMS collaboration, C. Collaboration, *Search for new physics in high mass diphoton events in  $3.3 \text{ fb}^{-1}$  of proton-proton collisions at  $\sqrt{s} = 13 \text{ TeV}$  and combined interpretation of searches at 8 TeV and 13 TeV*, .
- [15] L. Randall and R. Sundrum, *A Large mass hierarchy from a small extra dimension*, *Phys. Rev. Lett.* **83** (1999) 3370–3373, [[hep-ph/9905221](#)].
- [16] L. Randall and R. Sundrum, *An Alternative to compactification*, *Phys. Rev. Lett.* **83** (1999) 4690–4693, [[hep-th/9906064](#)].
- [17] K. Agashe, A. Delgado, M. J. May and R. Sundrum, *RS1, custodial isospin and precision tests*, *JHEP* **08** (2003) 050, [[hep-ph/0308036](#)].
- [18] K. Agashe, R. Contino, L. Da Rold and A. Pomarol, *A Custodial symmetry for  $Zb\bar{b}$* , *Phys. Lett. B* **641** (2006) 62–66, [[hep-ph/0605341](#)].
- [19] D. Guadagnoli, R. N. Mohapatra and I. Sung, *Gauged Flavor Group with Left-Right Symmetry*, *JHEP* **04** (2011) 093, [[1103.4170](#)].
- [20] C. S. Aulakh, A. Melfo and G. Senjanovic, *Minimal supersymmetric left-right model*, *Phys. Rev. D* **57** (1998) 4174–4178, [[hep-ph/9707256](#)].
- [21] P. Banerjee and U. A. Yajnik, *Production and decay rates of excited leptons in a left-right symmetric scenario*, *Phys. Rev. D* **90** (2014) 095023, [[1310.5785](#)].
- [22] S. K. Garg and C. S. Kim, *Vector like leptons with extended Higgs sector*, [1305.4712](#).
- [23] M. J. Dolan, J. L. Hewett, M. Krmer and T. G. Rizzo, *Simplified Models for Higgs Physics: Singlet Scalar and Vector-like Quark Phenomenology*, *JHEP* **07** (2016) 039, [[1601.07208](#)].
- [24] PARTICLE DATA GROUP collaboration, C. Patrignani et al., *Review of Particle Physics*, *Chin. Phys.* **C40** (2016) 100001.
- [25] Y. Zhang, H. An, X. Ji and R. N. Mohapatra, *General CP Violation in Minimal Left-Right Symmetric Model and Constraints on the Right-Handed Scale*, *Nucl. Phys. B* **802** (2008) 247–279, [[0712.4218](#)].
- [26] P. Langacker and S. U. Sankar, *Bounds on the Mass of  $W(R)$  and the  $W(L)$ - $W(R)$  Mixing Angle  $x_i$  in General  $SU(2)$ - $L \times SU(2)$ - $R \times U(1)$  Models*, *Phys. Rev. D* **40** (1989) 1569–1585.
- [27] R. Barbieri and R. N. Mohapatra, *Limits on Right-handed Interactions From SN1987A Observations*, *Phys. Rev. D* **39** (1989) 1229.

- [28] G. Beall, M. Bander and A. Soni, *Constraint on the Mass Scale of a Left-Right Symmetric Electroweak Theory from the  $K(L)$   $K(S)$  Mass Difference*, *Phys. Rev. Lett.* **48** (1982) 848.
- [29] G. C. Branco, J. M. Frere and J. M. Gerard, *The Value of  $\epsilon'/\epsilon$  in Models Based on  $SU(2)_l \times SU(2)_r \times U(1)$* , *Nucl. Phys.* **B221** (1983) 317–330.
- [30] G. Ecker, W. Grimus and H. Neufeld, *Higgs Induced Flavor Changing Neutral Interactions in  $SU(2)_l \times SU(2)_r \times U(1)$* , *Phys. Lett.* **B127** (1983) 365.
- [31] I. I. Y. Bigi and J. M. Frere, *Strong Radiative Corrections to Strangeness Changing Processes in the Presence of Right-handed Currents*, *Phys. Lett.* **B129** (1983) 469.
- [32] K. S. Babu, K. Fujikawa and A. Yamada, *Constraints on left-right symmetric models from the process  $b \rightarrow \bar{c} s$  gamma*, *Phys. Lett.* **B333** (1994) 196–201, [[hep-ph/9312315](#)].
- [33] P. Ball, J. M. Frere and J. Matias, *Anatomy of mixing induced CP asymmetries in left-right symmetric models with spontaneous CP violation*, *Nucl. Phys.* **B572** (2000) 3–35, [[hep-ph/9910211](#)].
- [34] A. Maiezza, M. Nemevsek, F. Nesti and G. Senjanovic, *Left-Right Symmetry at LHC*, *Phys. Rev.* **D82** (2010) 055022, [[1005.5160](#)].
- [35] M. Blanke, A. J. Buras, K. Gemmler and T. Heidsieck, *Delta  $F = 2$  observables and  $B \rightarrow X_q$  gamma decays in the Left-Right Model: Higgs particles striking back*, *JHEP* **03** (2012) 024, [[1111.5014](#)].
- [36] S. Bertolini, A. Maiezza and F. Nesti, *Present and Future K and B Meson Mixing Constraints on TeV Scale Left-Right Symmetry*, *Phys. Rev.* **D89** (2014) 095028, [[1403.7112](#)].
- [37] V. Bernard, S. Descotes-Genon and L. Vale Silva, *Short-distance QCD corrections to  $K^0 \bar{K}^0$  mixing at next-to-leading order in Left-Right models*, *JHEP* **08** (2016) 128, [[1512.00543](#)].
- [38] P. S. B. Dev, R. N. Mohapatra and Y. Zhang, *Probing the Higgs Sector of the Minimal Left-Right Symmetric Model at Future Hadron Colliders*, *JHEP* **05** (2016) 174, [[1602.05947](#)].
- [39] A. Joglekar, P. Schwaller and C. E. M. Wagner, *Dark Matter and Enhanced Higgs to Di-photon Rate from Vector-like Leptons*, *JHEP* **12** (2012) 064, [[1207.4235](#)].
- [40] K. Ishiwata and M. B. Wise, *Phenomenology of heavy vectorlike leptons*, *Phys. Rev.* **D88** (2013) 055009, [[1307.1112](#)].
- [41] R. Dermisek and A. Raval, *Explanation of the Muon  $g-2$  Anomaly with Vectorlike Leptons and its Implications for Higgs Decays*, *Phys. Rev.* **D88** (2013) 013017, [[1305.3522](#)].

- [42] N. Kumar and S. P. Martin, *Vectorlike leptons at the Large Hadron Collider*, *Phys. Rev.* **D92** (2015) 115018, [[1510.03456](#)].
- [43] A. Roitgrund, G. Eilam and S. Bar-Shalom, *Implementation of the left-right symmetric model in FeynRules*, *Comput. Phys. Commun.* **203** (2016) 18–44, [[1401.3345](#)].
- [44] A. Alloul, N. D. Christensen, C. Degrande, C. Duhr and B. Fuks, *FeynRules 2.0 - A complete toolbox for tree-level phenomenology*, *Comput. Phys. Commun.* **185** (2014) 2250–2300, [[1310.1921](#)].
- [45] A. Belyaev, N. D. Christensen and A. Pukhov, *CalcHEP 3.4 for collider physics within and beyond the Standard Model*, *Comput. Phys. Commun.* **184** (2013) 1729–1769, [[1207.6082](#)].
- [46] G. Blanger, F. Boudjema, A. Pukhov and A. Semenov, *micrOMEGAs4.1: two dark matter candidates*, *Comput. Phys. Commun.* **192** (2015) 322–329, [[1407.6129](#)].
- [47] PLANCK collaboration, P. A. R. Ade et al., *Planck 2013 results. XVI. Cosmological parameters*, *Astron. Astrophys.* **571** (2014) A16, [[1303.5076](#)].
- [48] WMAP collaboration, E. Komatsu et al., *Seven-Year Wilkinson Microwave Anisotropy Probe (WMAP) Observations: Cosmological Interpretation*, *Astrophys. J. Suppl.* **192** (2011) 18, [[1001.4538](#)].
- [49] XENON100 collaboration, L. Scotto Lavina, *Latest results from XENON100 data*, in *24th Rencontres de Blois on Particle Physics and Cosmology Blois, Loire Valley, France, May 27-June 1, 2012*, 2013. [1305.0224](#).
- [50] LUX collaboration, D. S. Akerib et al., *First results from the LUX dark matter experiment at the Sanford Underground Research Facility*, *Phys. Rev. Lett.* **112** (2014) 091303, [[1310.8214](#)].
- [51] XENON collaboration, E. Aprile et al., *Physics reach of the XENON1T dark matter experiment*, *JCAP* **1604** (2016) 027, [[1512.07501](#)].
- [52] T. Daylan, D. P. Finkbeiner, D. Hooper, T. Linden, S. K. N. Portillo, N. L. Rodd et al., *The characterization of the gamma-ray signal from the central Milky Way: A case for annihilating dark matter*, *Phys. Dark Univ.* **12** (2016) 1–23, [[1402.6703](#)].
- [53] FERMI-LAT, MAGIC collaboration, M. L. Ahnen et al., *Limits to dark matter annihilation cross-section from a combined analysis of MAGIC and Fermi-LAT observations of dwarf satellite galaxies*, *JCAP* **1602** (2016) 039, [[1601.06590](#)].
- [54] BAIKAL collaboration, A. D. Avrorin et al., *Search for neutrino emission from relic dark matter in the Sun with the Baikal NT200 detector*, *Astropart. Phys.* **62** (2015) 12–20, [[1405.3551](#)].

- [55] M. A. Shifman, A. I. Vainshtein, M. B. Voloshin and V. I. Zakharov, *Low-Energy Theorems for Higgs Boson Couplings to Photons*, *Sov. J. Nucl. Phys.* **30** (1979) 711–716.
- [56] J. F. Gunion, H. E. Haber, G. L. Kane and S. Dawson, *The Higgs Hunter’s Guide*, *Front. Phys.* **80** (2000) 1–404.
- [57] A. Djouadi, *The Anatomy of electro-weak symmetry breaking. II. The Higgs bosons in the minimal supersymmetric model*, *Phys. Rept.* **459** (2008) 1–241, [[hep-ph/0503173](#)].
- [58] A. Djouadi, *The Anatomy of electro-weak symmetry breaking. I: The Higgs boson in the standard model*, *Phys. Rept.* **457** (2008) 1–216, [[hep-ph/0503172](#)].
- [59] ATLAS collaboration, T. A. collaboration, *Measurement of fiducial, differential and production cross sections in the  $H \rightarrow \gamma\gamma$  decay channel with  $13.3 \text{ fb}^{-1}$  of 13 TeV proton-proton collision data with the ATLAS detector*, .
- [60] J. Alwall, R. Frederix, S. Frixione, V. Hirschi, F. Maltoni, O. Mattelaer et al., *The automated computation of tree-level and next-to-leading order differential cross sections, and their matching to parton shower simulations*, *JHEP* **07** (2014) 079, [[1405.0301](#)].
- [61] T. Sjostrand, S. Mrenna and P. Z. Skands, *PYTHIA 6.4 Physics and Manual*, *JHEP* **05** (2006) 026, [[hep-ph/0603175](#)].
- [62] DELPHES 3 collaboration, J. de Favereau, C. Delaere, P. Demin, A. Giammanco, V. Lematre, A. Mertens et al., *DELPHES 3, A modular framework for fast simulation of a generic collider experiment*, *JHEP* **02** (2014) 057, [[1307.6346](#)].
- [63] E. Conte, B. Fuks and G. Serret, *MadAnalysis 5, A User-Friendly Framework for Collider Phenomenology*, *Comput. Phys. Commun.* **184** (2013) 222–256, [[1206.1599](#)].
- [64] ATLAS collaboration, T. A. collaboration, *Measurement of the  $W^+W^-$  production cross section in pp collisions at a centre-of-mass energy of  $\sqrt{s} = 13 \text{ TeV}$  with the ATLAS experiment*, .
- [65] ATLAS collaboration, T. A. collaboration, *Electron efficiency measurements with the ATLAS detector using the 2015 LHC proton-proton collision data*, .
- [66] ATLAS collaboration, G. Aad et al., *Muon reconstruction performance of the ATLAS detector in protonproton collision data at  $\sqrt{s} = 13 \text{ TeV}$* , *Eur. Phys. J.* **C76** (2016) 292, [[1603.05598](#)].
- [67] D. Krohn, L. Randall and L.-T. Wang, *On the Feasibility and Utility of ISR Tagging*, [1101.0810](#).

- [68] V. Ari, O. Čakir and S. Kunday, *Pair Production of New Heavy Leptons with  $U(1)'$  Charge at Linear Colliders*, *Int. J. Mod. Phys. A* **29** (2014) 1450055, [[1309.7444](#)].
- [69] A. Vauth and J. List, *Beam Polarization at the ILC: Physics Case and Realization*, *Int. J. Mod. Phys. Conf. Ser.* **40** (2016) 1660003.
- [70] H. Baer, T. Barklow, K. Fujii, Y. Gao, A. Hoang, S. Kanemura et al., *The International Linear Collider Technical Design Report - Volume 2: Physics*, [1306.6352](#).